Title	NMR studies of metalloproteins
Author(s)	Li, H; Sun, H
Citation	Topics in Current Chemistry, 2012, v. 326, p. 69-98
Issued Date	2012
URL	http://hdl.handle.net/10722/142327
Rights	The original publication is available at www.springerlink.com

NMR studies of metalloproteins

Hongyan Li*, Hongzhe Sun

Department of Chemistry, The University of Hong Kong, Pokfulam Road, Hong Kong E-mail: hylichem@hku.hk

Abstract: Metalloproteins represent a large share of the proteomes, with the intrinsic metal ions providing catalytic, regulatory and structural role critical to protein functions. Structural characterization of metalloproteins and identification of metal coordination features including numbers and types of ligands and metal-ligand geometry, and mapping the structural and dynamic changes upon metal binding are of significance towards understanding biological functions of metallo-proteins. NMR spectroscopy has long been used as an invaluable tool for structure and dynamic studies of macromolecules. Here we focus on the application of NMR spectroscopy in characterization of metalloproteins, including structural studies, identification of metal coordination sphere by hetro-/homo-nuclear metal NMR spectroscopy. Paramagnetic NMR as well as ^{13}C directly detected proton-less NMR spectroscopy will also be addressed for paramagnetic metalloproteins. Moreover, these techniques offer great potentials in studies of other non-metal binding macromolecules.

Keywords: ^{13}C direct detection; metalloprotein; metal coordination; NMR spectroscopy; paramagnetic metalloprotein.

Contents

1 Introduction

Metal ions play important roles in life science and the molecular mechanism of metal-dependent life process and the entirety of metal within a cell or tissue/organ are the topics of emerging field of metallomics and metalloproteomics [1-3]. Metal ions usually must associate with proteins (and other biomolecules), i.e. metalloproteins, to prevent the toxic effects of metal excess. Metalloproteins are one of the most diverse classes of proteins with the intrinsic metal ions providing catalytic, regulatory and structural role critical to protein function, and are found in plants, animals and many microorganisms. It has been estimated that metalloproteins account for approximately one-quarter to one-third of all the proteins in the human body [4]. A recent study revealed that much of microbial metalloproteomes still remains uncharacterized [5]. Systematic bioinformatics survey on 1371 metalloenzymes with known structures showed that about 40% of enzyme-catalyzed reactions involve metal ions e.g. magnesium, zinc and iron [6]. Enormous efforts have been devoted toward understanding the structure and function of the metalloproteins and such knowledge was also used to design a new functional metalloprotein [7] and to rationalize and to search for new metalloproteins by bioinformatics approach [6, 8]. However, it is impossible currently from gene sequence to predict the numbers and types of metal an organism assimilates from its environment or uses in its metalloproteins because the geometry and composition of metal binding site are diverse and poorly-recognized [9, 10]. Therefore, understanding of the function of metalloproteins comes from individually characterization of the structures of the proteins and chemical states of the metal centers by various spectroscopic techniques including NMR spectroscopy, circular dichrosim (CD), elec-

tronic absorption spectroscopy (UV), small angle X-ray absorption as well as extended X-ray absorption fine structure (EXAFS).

Over the last three decades, NMR spectroscopy has been developed into a very important and versatile analytical technique both in the chemical and biological sciences. It has been used within the framework of Structural Genomic (SG) projects worldwide for determination of structures of proteins at atomic level under physiologically relevant conditions [11-13]. Moreover, NMR spectroscopy is applicable to study the interactions of proteins with other molecules including proteins, nuclei acids even small molecules which are mainly based on the sensitivity of the chemical shifts towards changes in the chemical environments [14, 15]. Application of this technique to structural studies is limited to small proteins (30-35 KDa) even with the aid of isotopic labeling (^{13}C, ^{15}N and ^{2}H) although backbone assignments of a 723-residue enzyme with a molecular weight of 81.4 KDa were achieved [16]. Recently, a few breakthroughs have been made in this field. This includes the first NMR structure of a seven-helix transmembrane protein determined in membrane-mimetic environments [17] and the first structure determined in living cells by in-cell NMR [18]. Apart from its application in structural studies, NMR spectroscopy is also able to monitor the internal motion of biomolecules ranging from subnanoseconds to beyond seconds. Characterization of dynamics of biomolecules, such as folding transition will be great help for our understanding the biological function of the biomolecules.

Application of NMR spectroscopy in studies of metalloproteins in principle is the same as other proteins if proteins contain diamagnetic metal ions. In the case of paramagnetic metalloproteins, things are getting more challenging since paramagnetic metals affect longitudinal and transverse relaxation rates of observed nuclei. However, recent advances in the hardware and methodology have enable structures of such metalloproteins to be determined including ^{13}C-detected experiments, solid-state NMR and discovery of paramagnetic relaxation enhancement (PRE) [19-21]. In this review, we will address mainly the application of NMR spectroscopy in studies of metalloproteins including contribution of NMR in structural characterization of metalloproteins, in particularly, special attention will be

devoted to utilization of NMR in characterization/identification of the metal binding sites and its coordination environment as well as in probing conformational changes of metalloproteins upon metal binding and release. The techniques used for paramagnetic metalloproteins will be also included briefly since a number of reviews in this field can be found [19-22]. Systematic review on application of metal NMR spectroscopy will not be made and interested readers are directed elsewhere [23].

2 The Contribution of NMR to structural metalloproteins

2.1 Conventional method for structure determination of metalloproteins

NMR spectroscopy can be applied to structurally characterize diamagnetic metal containing metalloproteins similarly as other proteins. Amongst the structures deposited to the Brookhaven Protein Data Bank (PDB), ca. 15% of the structures were resolved by NMR. Here, we will give a brief summary since the detailed methodology can be found in numerous references [11, 24-26].

In structural studies of proteins/metalloproteins, concentrations of about 1 mM are typically required and proteins must be soluble and stable over a period of time (weeks). For small proteins with several tens of amino acids e.g. metallothoinine [27, 28], it is sufficient using ^{15}N-labled samples to determine structures of the proteins. However, if proteins can be overexpressed in a bacterial system (e.g. *E. coli*), it is desirable to overexpress the protein with uniform enrichment of ^{15}N and ^{13}C even for small proteins. This will make full use of multidimensional heteronuclear NMR experiments to increase the spectral resolution. Unlike other proteins, expression of metalloproteins in a bacterial system usually requires specific metal ions to be supplemented in the medium to induce overexpression of the targeted proteins [14, 29]. Alternatively, metal ions have to be incorporated into the proteins after purification; in particular if the metal ions play structural roles, otherwise the proteins may not be stable for structural characterization. For example, HypA from *Helicobacter pylori* precipitates easily in the absence of zinc which serves a structural role [15]. However, caution has to be taken during metal incorporation since excess metal ions may also cause protein aggregation.

A major bottleneck in solving protein structures by NMR is the highly peak-picking and assignment of chemical shifts and NOEs. The strategy of assignment process and structure calculation can be found in an excellent review [30]. In general, for a $^{15}N/^{13}C$-labelled protein, a series of double/triple resonance experiments are recorded for resonance assignments. Backbone assignments are derived from HNCA, HNCOCA, HNCACB, CBCACONH, HNCO and HNCACO whereas side-chain protons and carbon atoms are assigned from HCCH-TOCSY, HCCH-COSY, HBHACONH, C(CO)NH and H(CCO)NH for [24, 25]. The chemical shifts of backbone and side-chain are then used to assign NOEs (^{15}N-/^{13}C-HSQC-NOESY) to derive inter-protein distance restraints. Usually structure determination process goes though several iterations of compiling a NOESY peak list, assignment of NOE cross-peaks to sequence-specific interactions, structure generations and assessment, refinement of NOESY peak lists and reassignment of the cross-peaks, which can be carried out automatically [31, 32]. In addition to distance restraints, dihedral angle restrains usually are obtained from several experiments e.g. HNHA [33], HNHB [34] or predicated from TALOS, a program that empirically predicts backbone angles (ϕ,Ψ) based on the chemical shifts of H^{α}, C^{α}, C^{β}, C´ and N [35], as well as the H-bond restraints derived from H-D exchange experiments. For an elongated macromolecules, RDC as an additional restraints is necessary for structure determination. Information about RDC can be found in Chapter 4 of this book. In order to get a relatively good quality of the structures, numbers of the NMR restraints used for structural determination are usually of the order of 10-20 independent interatomic distances per amino acid plus some dihedral restraints and as well as atom-atom vector directions. The quality of calculated structures has to be evaluated using programs PROCHECK, WHATIF etc. and detailed description can be found in a recent review [13].

In addition to general strategies described above, metal-based NMR parameters are also offering great help in evaluation of structures of metalloproteins especially for those metalloproteins that their folding is highly metal-dependent. To incorporate metal cluster constrains into structural calculation, residues that coordinate to metal ions (e.g. Zn^{2+}) must be identified first either by mutagenesis studies or

by physical characterization such as UV absorption spectroscopy, EXAFS and NMR spectroscopy [36-38]. Providing that metal coordination residues and geometries are unveiled, metal cluster restraints can be obtained based on relevant crystal structures of either macromolecules or small molecules. Usually, metal cluster restraints are not used in initial structure generation to avoid bias especially during the automated assignment procedure in CYANA [39], instead, metal ligand restraints are incorporated in the last step of structural calculation as well as in the refinement stage[40, 41].

The application of NMR spectroscopy in protein structure determination actually started with a small metalloprotein, metallothoinine (MT) [42]. Metallothoinines are a class of low molecular weight (typically 6-7 kDa) cysteine-rich proteins. The proteins are lack of well-defined secondary structure and their fold is dictated mostly by a clustered network of the cysteine residues and the metal ions usually represented by Zn^{2+}, Cu^{+} and Cd^{2+} [43, 44]. Since the first solution structure of rabbit liver Cd_7MT2 [42], numerous three dimensional structures of metallothiones from different isoforms (MT1/MT2/MT3) or different species such as blue crab and mammalian (rabbit, rat and human) have been resolved by NMR spectroscopy [45] with only one structure (rat liver Cd_5Zn_2MT2) determined by X-ray crystallography [46]. The protein consists two dynamic metal-thiolate clusters and folded into two domains (α, β) and structural mobility of the protein has made it difficult to be crystallized. The metal cluster restraints e.g. Cd-S bond lengths, as well as Cd-S-Cd, S-Cd-S and $CysC^{\beta}$-S-Cd bond angles from the X-ray crystal structures of model cadmium complexes and rat liver Cd_5Zn_2MT2 were often incorporated with other distance and angle restrains in structure calculation. Recently, a new member of metallothionine MT3 with the conserved CPCP motif in the N-termini is involved in the growth inhibitory activity and is down-regulated in the brain of Alzheimer's patients [47]. The solution structures of both human [27], and mouse MT3 [48] resolved by NMR spectroscopy for the C-terminal α-domain, Fig. 8.1a, revealed a similar Cd_4Cys_{11} cluster as well as a very similar tertiary folds to MT1/2. However, a loop in the acidic hexapeptide insertion is found and is slightly longer in human MT3 than in mouse MT3. The first

solution structure of Cd_7MT-nc of the Antarctic fish *Notothenia coriiceps* was also determined [28]. The position of the 9th cysteine of Cd_7MT-nc is different from mammalian MT which results in a structural change of the domain, in particular in the orientation of the loop (Lys50-Thr53), Fig. 8.1b, and in turn to a different charge distribution with respect to mammalian MT [28]. Interestingly, an intrigue class of histidine-containing metallothionines have also been identified in fungi and bacterial [49]. The histidine residue has been thought to be able to modulate zinc affinity and reactivity. Solution structure of one of this class of MTs, Zn_4SmtA from cyanobacterium *Synechococcus* PCC 7942 was determined [41], Fig. 8.1c, revealing a $Zn_4Cys_9His_2$ cluster with a topology similar to that of the Zn_4Cys_{11} cluster of the α-domain of mammalian MT. However, the two ZnCysHis sites and one of the $ZnCys_4$ site readily exchange Zn^{2+} for exogenous Cd^{2+}. Moreover, SmtA contains a short α-helix and two small antiparallel β-sheets surrounded the inert zinc site, which resemble zinc finger portions of GATA and LIM proteins. Such a structure of SmtA probably renders its function of specific protein and /or DNA recognition [41].

NMR spectroscopy has enormous contribution to structural biology of metalloproteins, particularly in zinc-binding proteins. Zinc, the second most abundant metal found in eukaryotic organisms, plays important catalytic and structural roles in variety biological processes. Binding of zinc is able to stabilize the folded conformations of domains, which renders a proper function of the protein [50]. Zinc finger proteins are the most abundant class of zinc-binding proteins that contain conserved cysteines and histidines coordinated to zinc. Intensive structural and functional studies have established the invariance of the ββα framework of the Cys_2His_2 zinc finger module and provided sound basis for understanding the nature of DNA recognition [40, 51-55]. Diverse structures of zinc fingers also account for their diverse functions such as DNA recognition, RNA packaging, transcriptional activation, regulation of apoptosis, protein folding and assembly as well as lipid binding [52, 56, 57]. Comprehensive reviews in this area can be found [56-58]. Here, we will only highlight some of the recent studies. Solution structure of Gfi-1 zinc finger 3-5 complex with a 16-mer consensus DNA

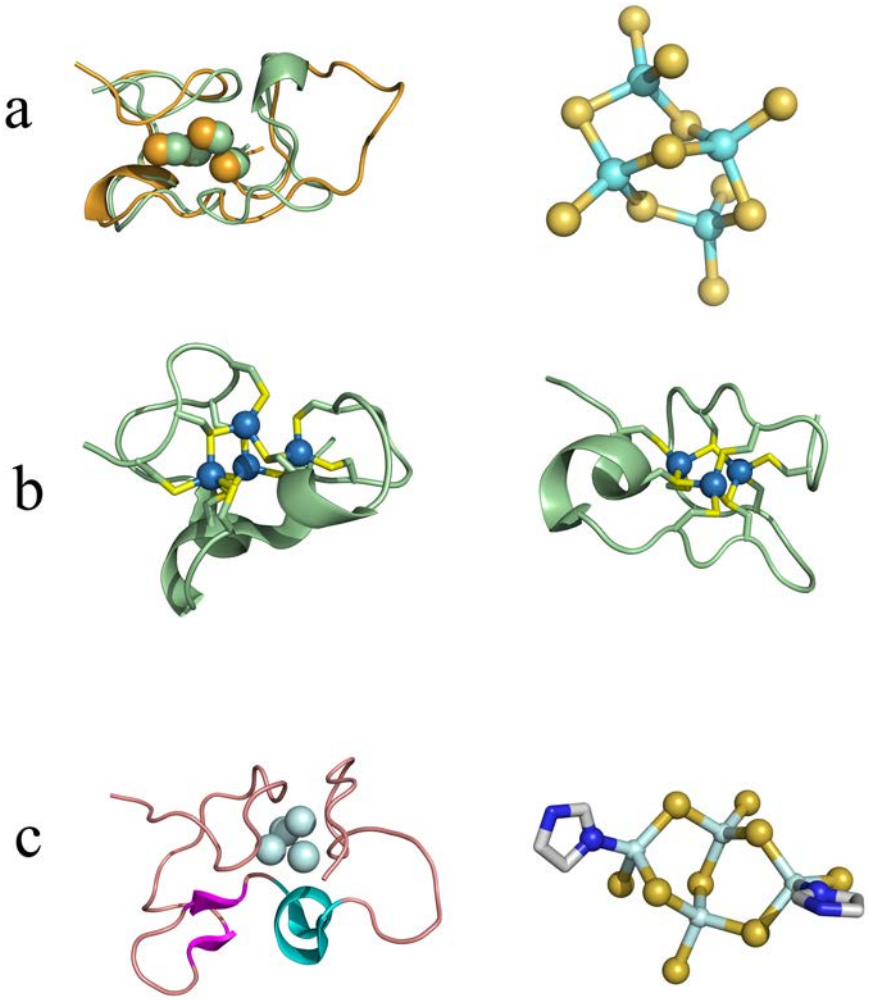

Fig. 8.1 (a) Overlaid view of structures of human MT3 (PDB: 2f5h) in orange and mouse MT3 (PDB: 1JI9) in pale green with the cadmium ions shown as spheres (left), and the four metal-thiolate cluster of human MT3 in the α-domain with the metal ions and sulfur atoms from cysteines shown in cyan and yellow respectively (right); (b) NMR structures of the *Notothenia coriiceps* Cd_7MT-nc with the α-domain (PDB: 1m0g) shown in the left and the β-domain (PDB: 1m0j) shown in the right. The metal thiolate clusters are also shown with the cadmium

ions shown as spheres in skyblue and sulfurs as sticks in yellow; (c) Solution structure of bacterial SmtA (PDB: 1jjd) with the zinc ions shown in pale cyan as spheres (left) and the metal cluster $Zn_4Cys_9His_2$ (right) with the zinc ions shown in pale cyan, sulfurs in yellow and the nitrogens of histidines in blue.

(Fig. 8.2a). Solution structure of Gfi-1 zinc finger 3-5 complex with a 16-mer consensus DNA (Fig. 8.2a) demonstrated zinc fingers 3-5 bind into the major groove of the target DNA reminiscent of canonical Cys_2His_2 zinc-finger domains, which provide valuable insight into the structure determinants for DNA binding specificity as well as molecular rationales for a naturally occurring mutation that causes acute myeloid leukemia [59]. Poly(ADP-ribose) (PAR) is an important post-translational modification in higher eukaryotes. Solution structures of two PBZ modules (PAR-binding zinc finger) of PNK-like factor (APLF) and the PDB domain of Drosophila melanogaster CG1218-PA reveal a novel type of Cys_2His_2 zinc finger and provide structural basis for PBZ-PAR recognition. Intriguingly, Cys_2His_2 zinc coordination of the PBZ modules is structurally and functionally dissimilar from canonical double stranded DNA-binding TFIIIA-type zinc finger, rather they resemble single-stranded RNA-binding Cys_3His_1 tandem zinc fingers (TZFs). Both of them are lack of secondary structures but have rigid backbone conformations as a result of zinc binding [60, 61]. Zinc finger proteins are also able to bind to RNA. The NMR structure of tandem zinc finger (TZF) domain of the protein TIS11d bound to the RNA sequence 5′-UUAUUUAUU-3′ (Fig. 8.2b) reveals a pair of novel Cys_3His_1 fingers which independently recognizes the four nucleotide sequence UAUU and the sequence specificity in RNA recognition is achieved by a network of intermolecular hydrogen bonds [62]. This structure provides insights into RNA-binding function of this family of Cys_3His_1 zinc finger proteins [62]. The Cys_3His_1 zinc finger motif is also found in the structure of SAP30 polypeptide of the Sin3 corepressor complex which adopts a novel fold comprising two β-strands and two α-helices with the zinc organized center. Such a structure may also function as a double-stranded DNA-binding motif [63]. The zinc finger CW (zf-CW) domain with a motif about 60 residues is frequently

found in proteins involved in epigenetic regulation. Interestingly, NMR structure of human zf-CW domain and PWWP domain containing proteins1 reveal a new fold in which a zinc is coordinated tetrahedrally by four conserved Cys residues [64]. Such a structure partially resembles the plant homeo domain (PHD) finger bound to the histone tail, implicating a similar function of zf-CW domain [64]. This kind of Cys_4 motif is widely found in other metalloproteins such as [NiFe] hydrogenases accessory protein HypA. Solution structure of HypA from *Helicobacter pylori* (Fig. 8.2c) showed that zinc coordinated to four cysteines donated from loops and no apparent secondary structure found in the zinc-domain [15]. The X-ray structure of HypA from *Thermococcus kodakaraensis KOD1* further confirmed such a zinc coordination sphere [65].

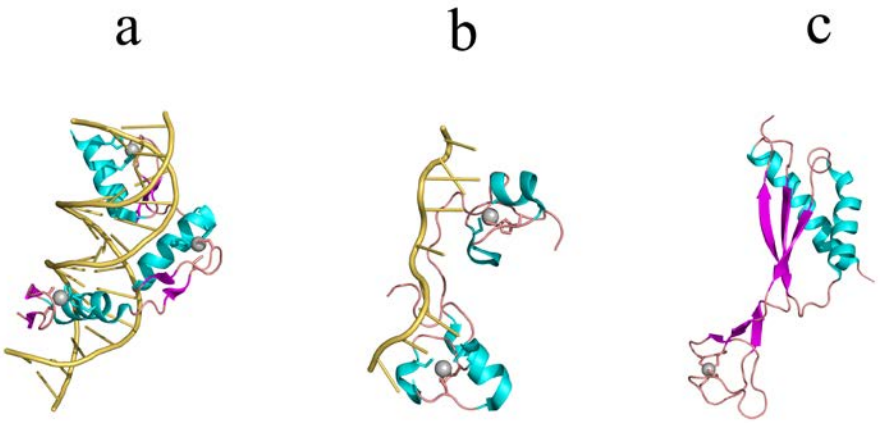

Fig. 8.2 (a) Ribbon diagram of the Gfizf35-DNA complex (PDB: 2kmk) with the zinc ions shown as gray spheres and the side-chains of two coordinated histidines and two cysteines shown in sticks and DNA shown in yellow sticks; (b) Solution structure of the RNA complex of TIS11d (PDB: 1rgo) with the zinc ions gray spheres coordinated to three cysteines and one histidine and RNA shown as yellow sticks; (c) Solution structure of HypA from *helicobacter pylori* (PDB: 2kdx) with the zinc ions in gray sphere coordinated to four cysteine sulfurs.

2.2 Utilization of chemical shifts to generate structures

Protein NMR chemical shifts are highly sensitive to local structure and reflect a wide array of structure factors including backbone and side-chain conformation, secondary structure, hydrogen bonds, and the orientation/ position of aromatic rings. Chemical shift data can be used in conjunction with protein sequence information and reasonable force field to generate 3D structure models using the method of CHEMSHIRE or CS-ROSETTA [66-68]. The Chemical-Shift-ROSETTA (CS-ROSETTA) is a robust protocol available for *de novo* protein structure generation. The method uses experimental chemical shifts of $^{13}C^{\alpha}$, $^{13}C^{\beta}$, $^{13}C'$, ^{15}N, $^{1}H^{\alpha}$, and $^{1}H^{N}$ as an input to select polypeptide fragments in existing protein structures (e.g. PDB data bank) in conjunction with the standard ROSETTA Monte Carlo fragment assembly and energy minimization protocol [67, 68]. The CS-ROSETTA has been further combined with CYANA using unassigned NOESY data to direct Rosetta trajectories toward the native structure and produces a more accurate models than CS-ROSEAAR alone [69]. Moreover, chemical shifts has been further extended in determination of protein-protein complex structures *via* CamDock method [70]. The method that utilizes chemical shifts to generate structures may provide potentially a new direction for high-throughput NMR structure determination of proteins including metalloprtoeins although such a method has not yet been applied in metalloproteins so far.

3 Identification of metal coordination

3.1 Homonuclear and hetronuclear metal NMR spectroscopy

Metalloprotein functionality depends on subtle interaction between properties of the metal ion, dictated by its coordination chemistry. Our present knowledge in terms of structure-function of metalloproteins in particular the role of metal ions involved varies considerably from proteins to proteins. Therefore, identification of metal coordination parameters including numbers and types of ligands and metal-ligand geometry and mapping the structural and dynamic changes upon metal binding are of significance towards understanding biological functions of metalloproteins. Today, NMR spectroscopy is one of the leading techniques for this pur-

pose. Applicability of homonuclear metal NMR and hetronuclear ^{1}H-metal HMQC to directly monitor protein-metal interactions highly rely on the properties of the nuclei. Some of the metal (e.g. ^{113}Cd) NMR has been used extensively to identify coordination sphere of the metal ions. Moreover, the coupling constants between the NMR active metals and nuclei of the protein provide insight into the identity and geometry of the metal ligands [71]. Many metal (e.g. ^{43}Ca, and ^{67}Zn) NMR are less powerful and hardly used owing to the fact that these nuclei have the spin quantum number *I* greater than ½ which led to lower sensitivity and poor resolution and broadening due to large quadrupolar moment although ultrahigh field improve it. Several reviews have systematically summarized the application of heteronuclear NMR spectroscopy in biological and medicinal chemistry as well as in study of metalloproteins [23, 71-73]. Here, we will highlight some of the recent progresses as a snapshot of using metal NMR to identify metal coordination.

Cadmium is one of the most widely used metal nuclei for probing metal-protein interactions, despite its toxic properties. It has two NMR active nuclei ^{113}Cd and ^{111}Cd (spins of ½) with the former being slightly more sensitive and therefore usually used as a preferred nucleus. At natural abundance, the sensitivity of ^{113}Cd is very low (*ca* 7.6 folds of ^{13}C), therefore isotopic enrichment (ca 96%) of ^{113}Cd is usually needed to ensure reasonable quality of spectra to be acquired in a relatively short period of time (few hours for *ca* 0.5 mM samples). ^{113}Cd or ^{113}Cd-^{1}H NMR spectroscopy has been utilized in the study of a variety of metalloproteins where the native Zn^{2+}, Ca^{2+}, Mg^{2+}, Mn^{2+}, Fe^{2+} and Cu^{2+} can be substituted by ^{113}Cd given that the adaptable ligand coordination number and geometry of Cd^{2+} is similar to Zn^{2+} and ionic radius of Cd^{2+} (0.97Å) is similar to that of Ca^{2+} (0.9 Å) [27, 74-77]. Moreover, the substitution of the native zinc from metalloenzymes and DNA-binding proteins by cadmium caused almost no changes in their structures and functions [78, 79].

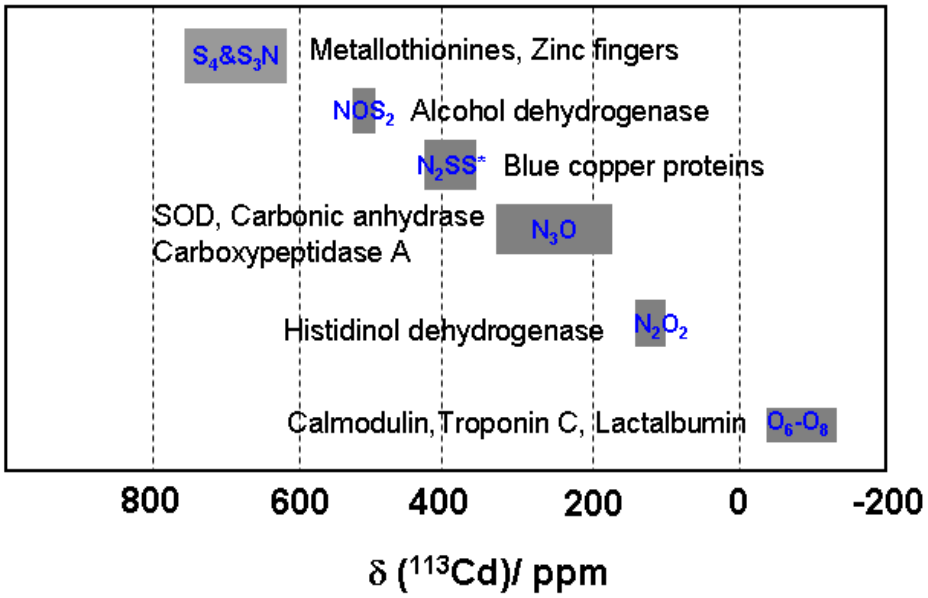

Fig. 8.3 Chemical shifts of ^{113}Cd for structurally characterized ^{113}Cd-substituted metalloproteins relative to external 0.1 M [$Cd(ClO_4)$]. The chemical shift positions are represented by gray bars and coordinating atoms are highlighted in blue with typical proteins listed besides. Here S represents sulfur from cysteine, S* represents sulfur from methionine, O represents oxygen from carboxylate or water and N represents nitrogen from histidine [71].

^{113}Cd chemical shifts are very sensitive to the nature, number, and geometric arrangement of the coordinated ligands [71] as shown in Fig. 8.3. Such wide chemical shift dispersion not only provides information about the types and numbers of ligand at a particular metal site, but also discriminates multiple metal sites with identical ligand coordination environments. ^{113}Cd NMR and ^{1}H-^{113}Cd HMQC has been employed exclusively in identification of metal-thiolate clusters in a family of small proteins *e.g.* metallothionines [27, 48, 71, 80]. Both homonuclear 1D ^{113}Cd decoupling studies (Fig. 8.4a) and 2D ^{113}Cd-^{113}Cd COSY (Fig. 8.4b) of $^{113}Cd_7$-MTs established the existence of two metal thiolate clusters in this protein, while ^{1}H-^{113}Cd HMQC (Fig. 8.4c) was used to identify sequence-specific cyste-

ine-cadmium coordination bonds. The chemical shift patterns for the two clusters Cd_3Cys_9 and Cd_4Cys_{12} of human MT3 as shown in Fig. 8.4a showed seven resonances at analogous position compared with MT1/2 with chemical shift ranging from 600 to 690 ppm [27]. However, the resonances from the α-domain (I, V, VI and VII) are slightly shifted in particular for resonance VII, probably attributed to the hexa-peptide insertion in this domain. The homonuclear 2D ^{113}Cd-^{113}Cd, Fig. 8.4b, clearly shows the correlation of cadmium signals which confirms the existence of two Cd-thiolate clusters [81]. The 2D ^{1}H-^{113}Cd HMQC as shown in Fig. 8.4c is normally used to obtain detailed metal-thiolate connectivity within each of these clusters [27]. Recently, metallothionines from different species such as sea mussel *Mytilus galloprovincialis* (Cd_7MT10) [81], and blue crab *Callinectes sapidus* (MTc) [82] have been studied by combined use of ^{113}Cd NMR, ^{113}Cd-^{113}Cd COSY and ^{1}H-^{113}Cd HMQC. Both proteins have 21 cysteine residues with position of cysteines distinct from mammalian MTs. The unique structure and dynamic features of the metal-thiolate cluster in these proteins are obviously seen from their distinct NMR parameters of Cd_7MTC [81, 82]. ^{111}Cd NMR has also been applied in studies of His-containing metallothionine, e.g. SmtA. The metal cluster of CdS_4 and CdN_2S_2 were identified [83], and ^{1}H-^{111}Cd HMQC of Cd_7SmtA unequivocally demonstrated couplings of two Cd^{2+} to both Hε1 or Hδ2 protons of two histidine residues [41]. Apart from metallothionines, cadmium NMR has also been employed to identify metal coordination environments in various metalloproteins, such as zinc finger [40] and [NiFe] hydrogenease accessory protein HypA [15], where in the latter case zinc ions (substituted by ^{113}Cd) are coordinated to four cysteine side-chins tetrahedrally. Moreover, it was also used to investigate major zinc binding site on human albumin [74, 84]. The chemical shifts of ^{111}Cd of human albumin (*ca*. 130 and 30 ppm) in combination with other techniques (EXAFS and mutagenesis studies) clearly demonstrated that the major zinc is five-coordinate site with residues of histidine and aspartate.

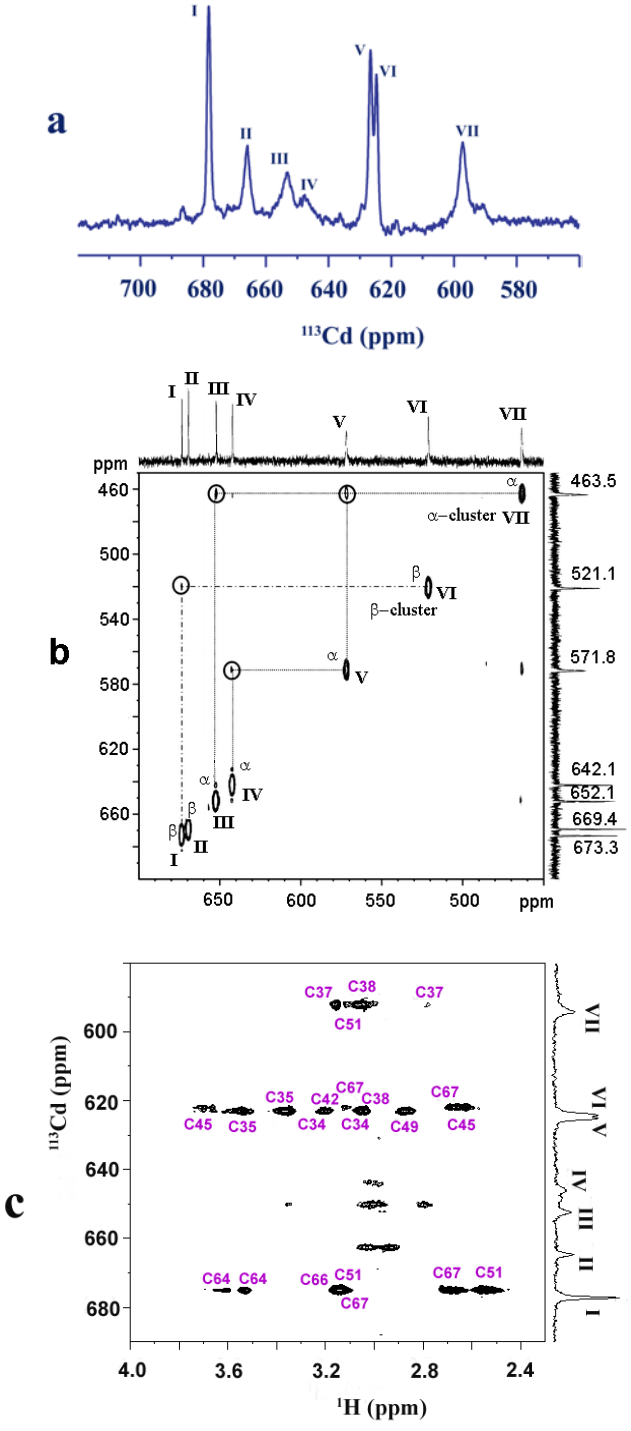
a
I
II
III
IV
V
VI
VII
700
680
660
640
620
600
580
113Cd (ppm)
b
ppm
α–cluster VII
β–cluster
463.5
521.1
571.8
642.1
652.1
669.4
673.3
650
600
550
500
ppm
c
C37
C38
C51
C35
C42
C67
C45
C34
C49
C64
C66
113Cd (ppm)
1H (ppm)
4.0
3.6
3.2
2.8
2.4

Fig. 8.4 (a) The 500 MHz NMR spectrum of human $^{113}Cd_7$-MT3 in 15 mM phosphate buffer, p H7.3 and 310 K. Resonances I, V, VI and VII are assigned to the α-domain and II, III and IV to the β-domain [27]. (b) 2D ^{113}Cd-^{113}Cd COSY NMR of Cd_7-MT10 in 17 mM Tris-d_{11} buffer, pH 7.0, 298 K with the one dimensional proton-decoupled ^{113}Cd NMR spectrum at the top. The cadmium connectivity in the α- and β-domains is also shown [81]. (c) The 500 MHz two-dimensional ^{1}H-^{113}Cd HMQC spectrum of human $^{113}Cd_7$-MT3 in 15 mM phosphate buffer with $^{3}J(^{1}H, ^{113}Cd)$ of 30 Hz. The assignments were also labeled with one-letter amino acid code [27].

Similarly, heteronuclear magnetic resonance spectroscopy with nuclei of spins ½ (e.g. $^{109}Ag/^{107}Ag$, ^{207}Pb and ^{199}Hg) has also been extensively employed in studies of metal coordination environments or the active site structures of metalloproteins. $^{109}Ag/^{107}Ag$ NMR has so far found limited application in biological systems due to low sensitivity and extremely long spin-lattice relaxation times. The only known metalloprotein studied by 2D ^{1}H-^{109}Ag HMQC spectroscopy to date is the silver-substituted yeast metallothionine [85]. The toxic lead (^{207}Pb), although it is not directly biological relevant, is an excellent substitute for Ca^{2+} in calcium-binding allowing them to retain similar structures and function. ^{207}Pb has a moderate resonance frequency, a vast chemical shift range (over thousands) and potentially large spin-spin coupling to neighboring nuclei which limits its application in study of metalloproteins. Although ^{207}Pb has been used to study active sites of model compounds or peptides of metalloenzymes [86, 87], there appears only one application using ^{207}Pb as a probe to study Pb^{2+} binding to the Ca^{2+} site of calcium-binding proteins including calmodulin (CaM) [88]. Binding of ^{207}Pb to both carp and pike parvalbumins gave rise to two ^{207}Pb signals from 750 to 1260 ppm downfield relative to aqueous $[Pb(NO_3)_2]$. Similarly, four ^{207}Pb signals, which fall in the same chemical shift window, could be observed for CaM. Both ^{207}Pb and ^{1}H have demonstrated that Pb^{2+} binds to all four sites simultaneously, in contrast to the behavior of the protein in the presence of Ca^{2+} [88]. The large chemical shift dispersion and remarkable sensitivity to chemical environment of ^{207}Pb signals

promote extensive studies using model complexes or peptides on mining the relationship of chemical shifts of ^{207}Pb with the numbers and types of coordinating ligands [86, 87, 89]. A recent study again demonstrated that chemical shifts of ^{207}Pb can be used to discriminate of PbS_3 (from Cys of thiolate-rich peptides) with other ligands such as PbS_3O and other O, S, and N donor ligands [89]. Therefore, based on ^{207}Pb chemical shift maps, Fig. 8.5a, both homonuclear and hetronuclear ^{207}Pb spectroscopy should provide a useful tool for investigation of Pb^{2+} coordination in more complex biological systems.

In spite of widely-known as protein-modifying agents, the toxic metal Hg^{2+} ion can be used as a probe to substitute the native metal ions for several metalloenzymes in a manner that preserves catalytic activity. Mercury has two NMR-active isotopes, ^{199}Hg and ^{201}Hg, with the latter having the spin of ½ and a natural abundance of 16.84%. ^{199}Hg exhibits several favorable NMR properties for structural and functional study, such as large coupling constants, and wide range of chemical shift dispersion (*ca*. 5000 ppm) and a relative sensitivity of 5.4 times of ^{13}C and 8 times of ^{113}Cd for an equal number of nuclei. Therefore, ^{199}Hg NMR techniques (^{199}Hg and ^{1}H-^{199}Hg HMQC) have been used as useful tools to probe the metal coordination environment in biological relevant complexes [90, 91] as well as regulatory proteins, copper enzymes, and zinc transcription factor complexes as large as 50 kDa [92-96]. The chemical shift of ^{199}Hg is very sensitive to the primary coordination spheres including numbers, types of ligands as well as coordination geometry. For examples, ^{199}Hg bound blue copper proteins gave rise to signals at ca -880 ppm for azurin and -749 ppm for plastocyanin and -706 ppm for rusticyanin [92, 95]. These blue proteins have very similar coordination environments e.g. two histidines and one cysteine and the fourth weakly associated ligand (Met or others) which is slightly different for these proteins. Nevertheless, such a subtle difference can be faithfully reflected by the chemical shifts of ^{199}Hg. The chemical shift map of ^{199}Hg can be derived based on various model complexes and proteins, Fig. 8.5b. The large chemical shift dispersion for ^{199}Hg allows clear differentiation between a variety of $M(SR)_n$ environments. Given that Hg^{2+} is readily exchanged for the native metal ion in many copper, zinc and iron metallo-

proteins [96], ^{199}Hg NMR methods can play an important role in structural, spectroscopic and chemical studies of metalloproteins and metal-binding domains where the tertiary structure of the folded proteins dictates the geometry of the metal ion.

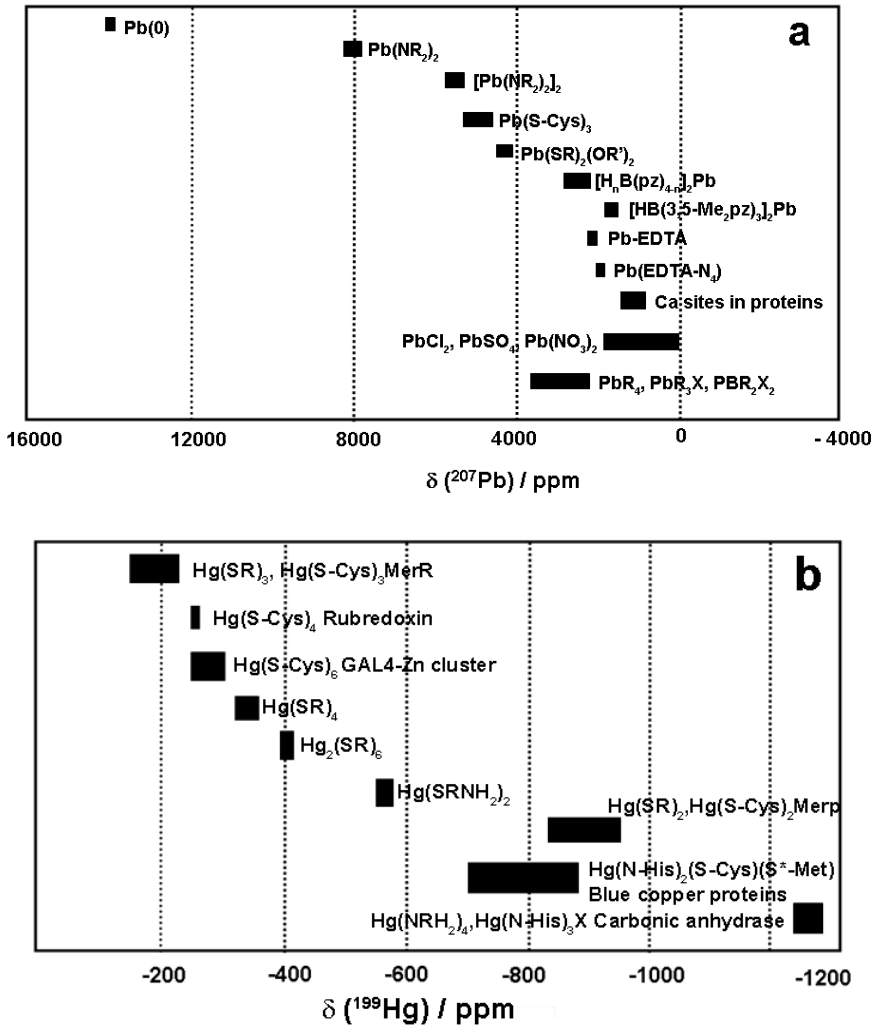

Fig. 8.5 (a) ^{207}Pb chemical shifts of various lead model complexes and ^{207}Pb-substituted proteins relative to external 1 M [$Pb(NO_3)_2$] in 99.9% D_2O pH* 3.3.

The pz represents Pyrazolyl ring and S-Cys represents a thiolate from cysteine (adapted from ref [87], [89]). (b) ^{199}Hg chemical shifts of aliphatic amine/thiol model complexes and ^{199}Hg-substituted proteins relative to $Hg(CH_3)_2$ at 298 K. The NRH_2 represents a primary amine and SR represents a thiolate, and the coordination environments of the Hg proteins include His imidazole nitrogen, Cys thiolate S-Cys and Met thioether S*-Met [94].

3.2 Chemical shift perturbation

Protein NMR chemical shift is highly sensitive to the exact environment of the atom and can provide valuable insights into structural features including metal ligation. For examples, chemical shifts of $^{13}C^{\beta}$ for the zinc bound cysteines (*ca*.34 ppm) are significantly downfield **Error! Bookmark not defined.**shifted relative to those of non-metal bound cysteines (*ca*. 27 ppm) [97]. Such an index has often been used to discriminate zinc bound cysteine residues [15, 98]. The chemical shift perturbations upon metal ion binding can be used to estimate the affinity, stoichiometry, and the kinetics of metal binding, and moreover it can be used to identify metal coordination environment. This approach is usually denoted as chemical shift mapping, which has been widely used to study protein-protein interaction [99, 100]. ^{1}H NMR and ^{1}H-^{1}H TOCSY have been used to identify the types of residues binding to metal ions for unlabeled small metalloproteins [101-103]. However, two dimensional HSQC especially ^{1}H -^{15}N HSQC is often employed in studies of metal coordination environment in metalloproteins due to the fact that it is well resolved in comparison with 2D ^{1}H -^{13}C HSQC. The identity of each cross-peak in the 2D ^{1}H -^{15}N HSQC spectra is assigned based on a series of triple resonance experiments. Binding of metal ions would lead to appearance of new peaks or disappearance of original peaks depending on the exchange rates of the apo- and metal-bound forms on the NMR time scales [99, 104]. The chemical shifts perturbation (CSP) can be followed in titration experiments, where the concentration of diamagnetic metal ion is increased gradually. When heteronuclear data are available, the binding site is usually predicated by the combined chemical shift perturbation $\Delta\delta_{comb}$, which has been showed to be a more reliable approach to

quantitative evaluate titration data [105]. Although several approaches are available to obtain this value as summarized previously [105], in practice, the weighting for ^{1}H and ^{15}N are considered to be the same, the $\Delta\delta_{comb}$ is usually quantified by the following equation:

$$\Delta\delta_{comb} = \sqrt{\frac{\Delta\delta_{HN}^2 + \frac{1}{25}\Delta\delta_{N}^2}{2}}$$

Chemical shift mapping provides information about the location of the metal-binding sites and has been used to identify the metal coordination for numerous metalloproteins [15, 106-108]. For examples, upon addition of Cu^{+} to human Cox17 induced significant chemical shift variations over residues Lys20 and Ala24, and the appearance of the NH signals of Cys22-Cys23, which is thought to serve as the Cu^{+} binding motif [107]. However, this approach usually has to be used in combination with other physical techniques or biological approaches e.g. mutagenesis to specify the metal binding sites since the chemical shift perturbations mainly stem from either direct binding or conformational changes caused by the metal ions. Binding of Ni^{2+} to *Helicobactor pylori* HypA led to disappearance of signals of Glu3 and Asp40 in the 2D ^{1}H-^{15}N HSQC spectrum. When combining with mutagenesis study, side-chain 2D ^{1}H-^{15}N HMQC, UV absorption as well as CD, it was proposed that Ni^{2+} coordinates with His2 (side-chain N^{δ}), His2 (backbone), Glu3 and Asp40 with a square-planar geometry [15]. Such a binding also induced structural changes which were thought to be important for its downstream receptor's recognition [15].

Histidine often serves as a metal binding ligand in metalloproteins and can provide both backbone and side nitrogens to coordinate with metal ions such as $Zn^{2+}$and Ni^{2+}. It has been shown that different tautomeric forms of histidine imadazole rings have different, distinguishable signal patterns in a long-range 2D ^{1}H-^{15}N HMQC spectrum [109] and metal coordination often causes recognizable changes in the NMR spectrum of histidine side-chains and that imadazole nitrogen atoms involved in direct metal coordination have specific chemical shift [15, 40, 98, 110]. This technique has been extensively used to identify Zn^{2+} binding. The

chemical shifts observed for the unprotonated imadazole nitrogen atoms of a zinc finger domain Hdm2(429-491) appeared at ca 215 ppm. The cross-peak pattern in ^{1}H-^{15}N HMQC spectrum (with $^{2}J_{HN}$) of zinc bound Hdm2 (429-491) showed that His452 and His457 assumed different tautomeric forms with the former being $N^{\varepsilon 2}$-protonated and the latter $N^{\delta 1}$-protonated with chemical shifts around 170 ppm, which demonstrated that Zn^{2+} coordinated to both His452 and His457 *via* the $N^{\varepsilon 2}$ and $N^{\delta 1}$ respectively [98]. More interestingly, a comparison of the 2D ^{1}H-^{15}N HMQC spectra of Zn^{2+}-bound proteins with $^{113}Cd^{2+}$-bound proteins, as shown in Fig. 8.6, allows one to observe the ^{15}N-^{113}Cd coupling, which assists identification of overlapping of histidine side-chains that binds to metal ions [40]. The HMQC spectrum of the zinc-bound domain, shown as black in Fig. 8.6a, clearly shows two of the ^{15}N resonances His42 and His40 shifted downfield as a result of zinc coordination. Based on the pattern of the cross-peaks, His42 is in the ε tautomeric state indicative of zinc coordination to the $N^{\delta 1}$ of His42, Fig. 8.6b. Such a method cannot be used to assign the nitrogen atom of His40 due to overlapping of the $H^{\delta 2}$ and $H^{\varepsilon 1}$ resonances of His40. The HMQC spectrum of ^{113}Cd bound protein, shown as red in Fig. 8.6a, clearly shows coupling between ^{113}Cd and the $N^{\delta 1}$ of His42 observed on $H^{\varepsilon 1}$, suggesting a covalent bond between them. Importantly, the pattern of the connectivities and the coupling observed to both $H^{\delta 2}$ and $H^{\varepsilon 1}$ from the ^{113}Cd allows the unambiguous assignment of the δ tautomer for His40, with the metal coordination via the $N^{\varepsilon 2}$ of the side-chain, Fig. 8.6b [40]. The side-chain 2D ^{1}H-^{15}N HMQC spectrum of histidine has also been used to identify Ni^{2+} binding atoms in *H. pylori* HypA and significant downfield shift of His2 upon Ni^{2+} binding indicates that Ni^{2+} binds to His2 through the $N^{\delta 1}$ atom [15].

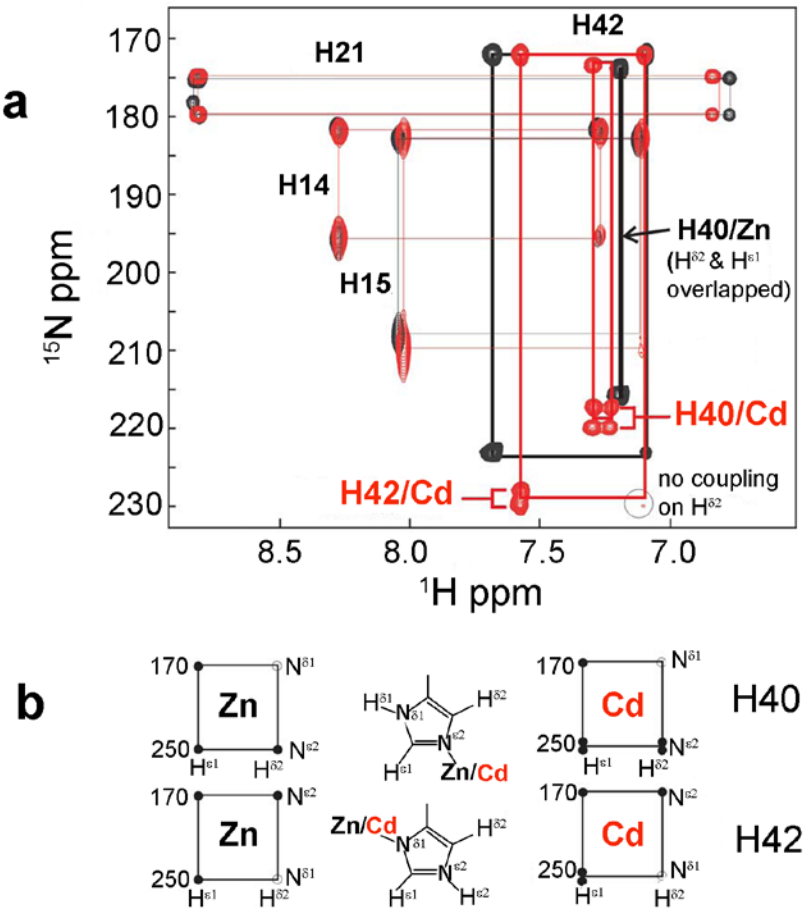

Fig. 8.6 (a) Comparison of the 500 MHz ^{1}H-^{15}N HMQC spectrum of Zn-bound ZZ domain in black with the ^{113}Cd-bound form in red. The coupling of ^{113}Cd to $N^{\varepsilon 2}$ is observed on $H^{\delta 2}$ and $H^{\varepsilon 2}$ for His40; whereas ^{113}Cd coupling to $N^{\delta 1}$ is observed on $H^{\varepsilon 1}$ for His 42. (b) Diagrams showing the connectivities of two zinc-ligand histidine residues H40 and H42 based on the above HMQC spectrum. The coupling of ^{113}Cd to the attached ^{15}N is useful for identification of metal bound histidine residues and the location of the metal coordination on the histidine rings (adapted from reference [40]).

4 NMR in studies of paramagnetic metalloproteins

Metalloproteins represent a large share of a proteome. A large number of them contains paramagnetic metal ions, which possess unpaired electrons. The presence of a paramagnetic centre causes pronounced effects in NMR spectra and reduces dramatically the intensity of NOEs and the efficiency in the transfer of scalar couplings both in homonuclear and heteronuclera experiments which hampers spectrum assignment and structural determination through standard approaches. However, , with the advances in novel experiment design and development of software protocol in recent years, the presence of paramagnetic centre has been used as a precious source of structural information [19, 20]. Extensive reviews regarding this topic can be referred to selected reviews [19-22, 111-113]. Here we will give a very brief description on the paramagnetism-based restraints as well as application of ^{13}C-detected experiments in structural of paramagnetic metalloproteins.

4.1 Paramagnetism-based structural restraints

In paramagnetic systems, where paramagnetic metal ions are either intrinsic or extrinsic, there are three NMR experimental observables that yield long-range structural information e.g. paramagnetic relaxation enhancement (PRE); pseudocontact shifts (PCS); residual dipolar couplings (RDC) induced by anisotropic paramagnetic centers. In addition, cross-correlated relaxation (CCR) effects between anisotropic paramagnetic centers and anisotropic parameters of the nuclear spins can also be exploited to generate long-range restraints [19, 111, 112]. Paramagnetic centers with isotropic electron spin distribution (Mn^{2+} and Gd^{3+}) produce large PREs due to slow electron relaxation. In contrast, paramagnetic centers with anisotropic electron spin distribution for most paramagnetic metal ions including most of the lanthanides create all four long-range paramagnetic effects, which contains rich structural information [114]. Here, we will focus on the PRE and PCS and their applications. Information about RDC can be found in Chapter 4.

The PRE arises from magnetic dipolar interactions between a nucleus and the unpaired electrons of the paramagnetic center, resulting in an increase in nuclear relaxation rates. In contrast to NOE, where the effects are limited to short

range interaction (< 6Å); the PRE effects are relatively large and can be detected up to 35 Å owing to large magnetic moment of an unpaired electron. There are two mechanisms e.g. the Solomon mechanism and the Curie spin mechanism that contribute the PREs, with the former being predominate for slowly tumbling molecules with long life-times of the electronic spin state (such as Mn^{2+} and Gd^{3+}). While the Curie relaxation becomes important when the electronic relaxation is much faster than the rotational tumbling of the molecules, which is the case for the majority of paramagnetic metal ions. Theoretical and experimental aspect of PRE as well as its application in studies of structures of proteins and protein-protein complexes can be found in recent reviews [114-116].

At high magnetic fields (over 500 MHz for ^{1}H frequency), the PRE rate, Γ_2 which arises from the dipole-dipole interaction between a nucleus and unpaired electrons with an isotopic *g*-tensor is conventionally calculated by the Solomon-Bloembergen (SB) equation:

$$\Gamma_2 = \frac{1}{15}\left(\frac{\mu_0}{4\pi}\right)^2 \gamma_I^2 g^2 \mu_B^2 S(S+1) r^{-6} \left\{ 4\tau_c + \frac{3\tau_c}{1+(\omega_H \tau_c)^2} \right\}$$

Where *r* is the distance between the paramagnetic centre and the observed nucleus; μ_0 is the permeability of vacuum; γ_I, the nuclear gyromagnetic ratio; *g*, the electron *g*-factor; μ_B, the electron Bohr magneton; S, the electron spin quantum number and τ_c, the PRE total correlation time. In practice, Γ_2 is measured as a difference in transverse relaxation rates between the paramagnetic ($R_{2,para}$) and diamagnetic ($R_{2,dia}$) states. A two-time point measurement is recommended as a simple approach of obtaining Γ_2 rates and their corresponding errors without fitting procedures. In this approach, the Γ_2 rates are determined from two time points (*T*=0 and *ΔT*) for transverse relaxation as shown by the following equation [116]:

$$\Gamma_2 = R_{2,para} - R_{2,dia} = \frac{1}{T_b - T_a} \ln \frac{I_{dia}(T_b) I_{para}(T_a)}{I_{dia}(T_a) I_{para}(T_b)}$$

Where I_{dia}, I_{para} are the peak intensities for the diamagnetic and paramagnetic states, respectively. The choice of time points is important to minimize the error.

For example, if the range of Γ_2 rates is 0-75 s^{-1}, a second time point Tb should be at *ca.* 1.15/($R_{2,dia}$+50) s, represent a reasonable choice [115, 116].

For isotropic metal ions such as Mn^{2+} and Gd^{3+}, the Curie-spin relaxation that could potentially exhibit significant cross-correlation with other relaxation mechanisms, is negligible for medium-size macromolecules [116], the Solomon relaxation is predominant. PRE analysis in such a system is thus simple. The PRE has been used extensively in metalloproteins that possess a rigid intrinsic paramagnetic center [117-119]. Such a strategy has also been extended not only in the NMR structure determination of non metalloproteins [120-122], in which paramagnetic metal ions (Mn^{2+} or Gd^{3+}) or nitroxide radicals were conjugated through appropriate chemical modification [123], but also in the characterization of protein-protein/nuclei acid complexes [124-126]; and membrane-proteins [127], in particular in transient macromolecular interactions [115, 128-131].

Pseudocontact shifts (PCSs) are precious source of structure information and observed only in paramagnetic systems with anisotropic unpaired electrons e.g. Dy^{3+}, Tb^{3+} and Fe^{3+}. The magnitude of the PCS, δ^{pcs}, is calculated using the following equation [132]:

$$\delta^{pcs} = \frac{1}{12\pi} r^{-3} \left\{ \Delta\chi_{ax} (3\cos^2\theta - 1) + \frac{3}{2} \Delta\chi_{rh} \sin^2\theta \cos 2\varphi \right\}$$

$$\Delta\chi_{ax} = \Delta\chi_{zz} - \frac{1}{2}(\chi_{xx} + \chi_{yy}) \text{ and } \Delta\chi_{rh} = \chi_{xx} - \chi_{yy}$$

Where r is the distance between the metal ion and the nuclear spin; θ and φ are the angles describing the position of the nuclear spin with respect to the principle axes of the magnetic susceptibility tensor χ; and the $\Delta\chi_{ax}$ and $\Delta\chi_{rh}$ are the axial and rhombic components, respectively, of the magnetic susceptibility tensor.

The PCS are manifested by large changes in chemical shifts of the nuclear spins that are exposed to the paramagnetic metal ions and arise from through-space dipolar interactions with rapidly relaxing unpaired electrons. The PCS displays a r^{-3} distance dependence, in contrast to the r^{-6} dependence for the PRE,

which results in a relatively long distance range for the PCS to be detected (*ca*. 40 Å for Dy^{3+}) [133]. In general, the δ^{pcs} values can be measured after the complete assignment for the ^{1}H-^{15}N HSQC spectra of the both the diamagnetic and the paramagnetic samples is obtained and is calculated as the difference between the chemical-shift values observed for the nuclei in a paramagnetic system and in a diamagnetic analogue. The δ^{pcs}-derived restrains alone can not be used to solve the structures. Instead, the PCSs have to be incorporated with NOEs and dihedral-angle restraints to determine structures of proteins or to refine protein structures. The first example of using PCS in a structure refinement was reported on a low-spin Fe^{3+} heme protein [134]. Such a strategy has been extended not only in studies of paramagnetic proteins [135, 136], but also in non-metal binding proteins [137, 138], which were labeled by paramagnetic metal ions such as lanthanides [114, 139], or genetically encoded Co^{2+}-binding amino acid [140]. Moreover, PCSs can also be used as restraints in molecular dynamics [141, 142].

4.2 ^{13}C-detected protonless NMR

Direct-detection of heteronuclei, in particular ^{13}C offers a valuable alternative to ^{1}H detection in the study of biological macromolecules [143-145] as well as paramagnetic proteins [136, 145-147]. The recent development of high magnetic fields as well as the availability of cryogenically cooled probe-heads has improved ^{13}C sensitivity significantly, which greatly stimulated research of using ^{13}C-detected experiments on enriched samples to study biological macromolecules [148]. The ^{13}C detection takes advantage of the slower relaxing ^{13}C spins and overcomes the drawbacks produced by the fast ^{1}H transverse relaxation, which led ^{1}H signals broaden beyond detection limits for large proteins. Such an approach is particularly useful in paramagnetic systems since ^{13}C direct detection is less affected by the paramagnetic center than ^{1}H owing to the lower ^{13}C gyromagnetic ratio, which decreases the paramagnetic dipolar contributions to its relaxation by a factor of around 16 $(\gamma_C/\gamma_H)^2$ [136, 146, 149].

In ^{13}C direct-detection experiments, several approaches were used to achieve “virtual” decoupling (to remove homonuclear one-bond carbon-carbon couplings)

such as IPAP schemes (in-phase anti-phase) [150-152], in which two FIDs for each increment are recorded and stored separately, one for in-phase and another for anti-phase and two components are combined to remove the splitting; or S^3E schemes [152, 153] (spin-state selective excitation), in which two different experiments are performed with one being absortive and another dispersive. One or more of these building blocks (IPAP and S^3E) can be implemented in any experiments based on ^{13}C direct-detection. A set of ^{13}C based experiments, which can be used for the assignment of backbone and side-chains of $^{13}C/^{15}N$ labeled proteins, are now available and summarized in a recent review [144]. The sequence-specific assignment was achieved by CACO and CANCO, which provide the correlation of each CO to the two neighboring C^{α} nuclei; CACO, CBCACO and ^{13}C-^{13}C TOCSY can provide spin-system assignment [143, 154, 155]. The CON-IPAP experiment is used to correlate backbone nitrogen with CO through the one-bond C′-N coupling [149]. The ^{13}C-^{13}C NOESY experiments based on dipole-dipole interaction with longitudinal magnetization transfer represent a valuable alternative to COSY experiments based on scalar couplings to detect C-C one bond correlation for large macromolecules and paramagnetic metalloproteins [149, 156, 157]. The ^{13}C-^{13}C NOESY with direct ^{13}C detection is exploited as a valuable tool to extend the assignment to side-chains in large molecules such as C´-C^{β} if mixing times is long enough (e.g. 800 ms) [156]. The correlations between nuclei not directly bound and not mediated by spin diffusion in ^{13}C-^{13}C NOESY spectra are identified, which would represent a breakthrough of structure determination of large macromolecules in solution by providing distance constraints. However, the sensitivity for ^{13}C direct detection is required to be improved before long-rang correlations to obtain ^{13}C-^{13}C distance constraints can be used in structural characterization of large macromolecules.

^{13}C direct detection has been successfully applied to paramagnetic proteins, where the contribution to line broadening coming from the paramagnetic centre is so large that ^{1}H signals around the metal ion is beyond detectable limits [136, 144, 147, 149, 158]. Such a technique can also be used in generation of paramagnetism-based restraints including PCS, PRE, RDC [148, 159-161]. It has been dem-

onstrated that ^{13}C directly detected spectra provide an alternative method for the measurement of RDC with precision as good as that from ^{1}H detection, but with additional advantage for measuring those broad resonances in ^{1}H detection [148]. Direct-detection of ^{13}C intrinsically offers a way to detect resonances close to the metal ion where ^{1}H resonances are too broad to be detected. Indeed, with the aid of ^{13}C direct detection approach, ^{13}C resonances as close as 6 Å from the metal ion are detected for CopC, a Cu^{2+} binding protein involved in copper homeostasis, whereas no ^{1}H resonance can be detected in a sphere of 11 Å from the metal due to fast relaxation caused by paramagnetic Cu^{2+} [136]. Incorporation of heteronuclear paramagnetism-based restraints e.g. PCSs and longitudinal relaxation rate enhancement allows CopC structures to be resolved with the RMSD of Cu^{2+} determined only by the paramagnetism-based constraints of 1.1 Å [136]. ^{13}C direct detection technique has also been used for residue-specific assignments of resonances, in particular those near paramagnetic centers (e.g. Ni^{2+}, Fe^{3+}) such as in a 20 kDa Ni-containing enzyme, acireductone dioxyhenase (ARD) [162] and oxidized human [2Fe-2S] ferredoxin [146], as well as a 19 kDa Fe^{3+} hemophore HasA [147]. In many paramagnetic systems, the longitudinal relaxation rates are influenced to a smaller extent than the transverse relaxation rates. The ^{13}C-^{13}C NOESY experiments are therefore a useful approach to overcome the quench of scalar coupling based transfer in particular for large macromolecules. The use of ^{13}C direct detected experiments e.g. ^{13}C-^{13}C COSY, ^{13}C-^{13}C NOESY and ^{13}C-^{13}C COCAMQ allows ^{13}C signals as close as 4 Å to Cu^{2+} to be detected in oxidized monomeric copper, zinc superoxide dismutase (SOD) [149]. The advantage of ^{13}C-^{13}C NOESY experiments for higher molecular weights was seen by comparison of the protein SOD [149, 156]. All of the expected Cα-CO connectivities were detected with higher intensity in the dimeric protein than in the monomeric state. In addition, most of the two bond CO-Cβ cross-peaks were observable for the dimeric SOD when the long mixing times were used [156]. Interestingly, the intrinsic asymmetry of a ^{13}C-^{13}C COSY experiment allows the coordinating residues of a paramagnetic metal ions to be identified easily, provides a unique method to distinguish between monodentate and bidentae coordinating side-chain carbonyls

[163]. Significantly, the ^{13}C-based strategy in combination with solid-state NMR led to partial sequence-specific (35%) and side-chain assignments for the iron storage protein, ferritin, a very large protein with a molecular mass of 480 kDa and 24-subunits [164, 165]. The solution ^{13}C-^{13}C NOESY spectra for side-chain observation has provided the identification of an iron channel that guides the direction transport of the multimeric Fe^{3+} products from the active site toward the nanocage. The interior of the four-helix bundle is identified as the functional channel based on the observed paramagnetic effects on residues lining the internal face of the four-helix bundle. The NMR data provide a basis for the pathway of iron from the ferrous/dioxygen oxidoreductase site to the central cavity of ferritin [164]. Such studies open new avenues for the application of ^{13}C direct detection experiments to systems with molecular assemblies larger than 100 kDa.

5 Perspectives

Since the first protein solution structure was determined by high resolution NMR spectroscopy about 25 years ago [166], NMR has been established as the only experimental method that provides both structural and dynamical information at atomic resolution close to physiologically relevant conditions. Protein structure determination in living cells has also been achieved recently by in-cell NMR [18]. However, the limitation of this technique in structural studies lies in low sensitivities and poor resolution when the size of macromolecules increases. Some proteins, in particular metalloproteins might not be stable for a period of time (days or weeks) or have limited solubility. Moreover, new challenges in life science has also promoted development of new NMR methods which will improve sensitivities and reduce acquisition times to fulfill the requirement of characterization of these proteins and their complexes.

Enormous effort has been made to improve NMR instrumentation in terms of experimental sensitivity, which results in availability of high-field magnets, cryogenically cooled probes. In the meantime, tremendous advances in methodology have contributed to an increased interest in the study of molecular systems of increasing size and complexity. The introduction of non-linear sampling scheme (in-

stead of conventional uniform sampling) allows a very fast acquisition of multi-dimensional NMR [167-169]. Many schemes have been developed to reduce the spectral dimensionality, thus to speed up the experiments, which enable quick assignment of large proteins [170, 171]. The examples include "GFT" NMR approach where sub-spectra from joint sampling of indirect dimensions are linearly recombined and analyzed [172]. In projection reconstruction ("PR") method, the corresponding full-dimensional spectrum is reconstructed [171, 173, 174]. Moreover, various ultrafast NMR techniques including SOFAST/BEST NMR [175, 176] and Hadmard NMR [177] are also available for studies events of biomolecules even in real time. All these new schemes deliver appreciable improvement in the speed of data acquisition and show promise for speed up multidimensional NMR of normal size proteins [170, 178, 179] and very large proteins [180, 181] as well as sequence assignment for intrinsically unstructured proteins [178].

^{13}C NMR spectroscopy is emerging as a powerful tool to complement ^{1}H NMR spectroscopy in the investigation of biomolecules, in particular for large molecules and paramagnetic metalloproteins and also for the study of short-lived molecules [182]. However, the data acquisition time is rather long even for sample with high concentrations (*ca*. mM). Implementation of fast NMR methods such as non-uniform sampling in the indirect dimension significantly reduced experimental times [183]. Such a strategy will open new avenues to applications of ^{13}C NMR to take advantage of the favorable heteronuclear chemical shift dispersion in biological systems especially for systems of increasing size.

Chemical shifts of selective nuclei ($^{113/111}$Cd, ^{209}Pb, ^{195}Pt) are sensitive towards types of ligands (N, O and S), numbers and geometries, and will continue to play a role in characterization of metal-protein local coordination. The ultra-field NMR facilities direct observation of biologically important metal ions with half integer, quadrupolar nuclei (e.g. ^{67}Zn and ^{25}Mg) [184, 185] .

In spite of availability of all these new techniques, their applications in metalloproteins are currently sparse. There is an urgent need to promote these advanced techniques in the scientific community through introducing integrated software packages for experimental set-up, data processing and analysis. This will enable

protein chemists and bioinorganic chemists, who are not NMR experts, to employ the new techniques in their research. The combination of fast NMR techniques, ^{13}C directly detected NMR with paramagnetic NMR will offer great potentials in tackle new challenges in life science and open new avenues for NMR spectroscopy to be utilized not only in the characterization of single biomolecules e.g. structural and dynamical studies of proteins/metalloproteins and paramagnetic proteins, short-lived macromolecules and intrinsically unstructured proteins, but also in investigation of more complex systems to give an integrated view of interacting molecular networks. In particular, the ultra-fast NMR opens new perspectives for the NMR structural investigation of unstable protein/metalloprotein samples and real-time site-resolved studies of protein kinetics or monitoring folding/unfolding processes of proteins/metalloproteins caused by ligand or metal binding/release.

Acknowledgements

This work is supported by the Research Grants Council of Hong Kong (HKU7043/06P, HKU2/06C, HKU7042/07P, HKU1/07C, HKU7038/08P, HKU7049/09P and N-HKU752/09), Croucher Foundation.

Reference

1. Ge R, Sun X, Gu Q et al (2007) A proteomic approach for the identification of bismuth-binding proteins in Helicobacter pylori. J Biol Inorg Chem 12: 831-842
2. Sun XS, Tsang CN, Sun HZ (2009) Identification and characterization of metallodrug binding proteins by (metallo)proteomics. Metallomics 1: 25-31
3. Sun HZ, Chai ZF (2010) Metallomics: An integrated science for metals in biology and medicine. Annu. Rep. Prog. Chem., Sect. A: Inorg. Chem. 106: 20-38
4. Waldron KJ, Robinson NJ (2009) How do bacterial cells ensure that metalloproteins get the correct metal? Nat Rev Microbiol 7: 25-35
5. Cvetkovic A, Menon AL, Thorgersen MP et al (2010) Microbial metalloproteomes are largely uncharacterized. Nature 466: 779-782
6. Andreini C, Bertini I, Cavallaro G et al (2008) Metal ions in biological catalysis: from enzyme databases to general principles. J Biol Inorg Chem 13: 1205-1218
7. Lu Y, Yeung N, Sieracki N et al (2009) Design of functional metalloproteins. Nature 460: 855-862
8. Andreini C, Bertini I, Rosato A (2009) Metalloproteomes: a bioinformatic approach. Acc Chem Res 42: 1471-1479

9. Shu N, Zhou T, Hovmoller S (2008) Prediction of zinc-binding sites in proteins from sequence. Bioinformatics 24: 775-782
10. Kasampalidis IN, Pitas I, Lyroudia K (2007) Conservation of metal-coordinating residues. Proteins 68: 123-130
11. Wuthrich K (1989) Protein structure determination in solution by nuclear magnetic resonance spectroscopy. Science 243: 45-50
12. Montelione GT, Arrowsmith C, Girvin ME et al (2009) Unique opportunities for NMR methods in structural genomics. J Struct Funct Genomics 10: 101-106
13. Banci L, Bertini I, Luchinat C et al (2010) NMR in structural proteomics and beyond. Prog Nucl Magn Reson Spectrosc 56: 247-266
14. Wang H, Li H, Cai B et al (2008) The effect of nitric oxide on metal release from metallothionein-3: gradual unfolding of the protein. J Biol Inorg Chem 13: 411-419
15. Xia W, Li H, Sze KH et al (2009) Structure of a nickel chaperone, HypA, from *Helicobacter pylori* reveals two distinct metal binding sites. J Am Chem Soc 131: 10031-10040
16. Tugarinov V, Muhandiram R, Ayed A et al (2002) Four-dimensional NMR spectroscopy of a 723-residue protein: chemical shift assignments and secondary structure of malate synthase g. J Am Chem Soc 124: 10025-10035
17. Gautier A, Mott HR, Bostock MJ et al (2010) Structure determination of the seven-helix transmembrane receptor sensory rhodopsin II by solution NMR spectroscopy. Nat Struct Mol Biol 17: 768-774
18. Sakakibara D, Sasaki A, Ikeya T et al (2009) Protein structure determination in living cells by in-cell NMR spectroscopy. Nature 458: 102-105
19. Bertini I, Luchinat C, Parigi G et al (2005) NMR spectroscopy of paramagnetic metalloproteins. ChemBioChem 6: 1536-1549
20. Bertini I, Luchinat C, Parigi G et al (2008) Perspectives in paramagnetic NMR of metalloproteins. Dalton Trans: 3782-3790
21. Bertini I, Luchinat C, Piccioli M (2001) Paramagnetic probes in metalloproteins. Methods Enzymol 339: 314-340
22. Bertini I, Luchinat C (1999) New applications of paramagnetic NMR in chemical biology. Curr Opin Chem Biol 3: 145-151
23. Ronconi L, Sadler PJ (2008) Applilcations of heteronuclear NMR spectroscopy in biological and medicnal inorganic chemistry. Coord Chem Rev 252: 2239-2277
24. Rule GS, Hitchens TK (2006) *Fundamentals of protein NMR spectroscopy*. Springer, Netherlands
25. Clore GM, Gronenborn AM (1999) In: Krishna NR, Berliner LJ (ed) Biological Magnetic Resonance. Kluwer Academic/Plenum Publishers, New York
26. Wuthrich K (2003) NMR studies of structure and function of biological macromolecules (Nobel lecture). Angew Chem Int Ed Engl 42: 3340-3363
27. Wang H, Zhang Q, Cai B et al (2006) Solution structure and dynamics of human metallothionein-3 (MT-3). FEBS Lett 580: 795-800

28. Capasso C, Carginale V, Crescenzi O et al (2003) Solution structure of MT_nc, a novel metallothionein from the Antarctic fish Notothenia coriiceps. Structure 11: 435-443
29. Ge R, Watt RM, Sun X et al (2006) Expression and characterization of a histidine-rich protein, Hpn: potential for Ni^{2+} storage in *Helicobacter pylori*. Biochem J 393: 285-293
30. Williamson MP, Craven CJ (2009) Automated protein structure calculation from NMR data. J Biomol NMR 43: 131-143
31. Guntert P (2009) Automated structure determination from NMR spectra. Eur Biophys J 38: 129-143
32. Lopez-Mendez B, Guntert P (2006) Automated protein structure determination from NMR spectra. J Am Chem Soc 128: 13112-13122
33. Kuboniwa H, Grzesiek S, Delaglio F et al (1994) Measurement of HN-H alpha J couplings in calcium-free calmodulin using new 2D and 3D water-flip-back methods. J Biomol NMR 4: 871-878
34. Dux P, Whitehead B, Boelens R et al (1997) Measurement of (15)N- (1)H coupling constants in uniformly (15)N-labeled proteins: Application to the photoactive yellow protein. J Biomol NMR 10: 301-306
35. Cornilescu G, Delaglio F, Bax A (1999) Protein backbone angle restraints from searching a database for chemical shift and sequence homology. J Biomol NMR 13: 289-302
36. Cun S, Sun H (2010) A zinc-binding site by negative selection induces metallodrug susceptibility in an essential chaperonin. Proc Natl Acad Sci U S A 107: 4943-4948
37. Scrofani SD, Wright PE, Dyson HJ (1998) The identification of metal-binding ligand residues in metalloproteins using nuclear magnetic resonance spectroscopy. Protein Sci 7: 2476-2479
38. Bordiga S, Bonino F, Lillerud KP et al (2010) X-ray absorption spectroscopies: useful tools to understand metallorganic frameworks structure and reactivity. Chem Soc Rev 39: 4885-4927
39. Herrmann T, Guntert P, Wuthrich K (2002) Protein NMR structure determination with automated NOE assignment using the new software CANDID and the torsion angle dynamics algorithm DYANA. J Mol Biol 319: 209-227
40. Legge GB, Martinez-Yamout MA, Hambly DM et al (2004) ZZ domain of CBP: an unusual zinc finger fold in a protein interaction module. J Mol Biol 343: 1081-1093
41. Blindauer CA, Harrison MD, Parkinson JA et al (2001) A metallothionein containing a zinc finger within a four-metal cluster protects a bacterium from zinc toxicity. Proc Natl Acad Sci U S A 98: 9593-9598
42. Arseniev A, Schultze P, Worgotter E et al (1988) Three-dimensional structure of rabbit liver [Cd7]metallothionein-2a in aqueous solution determined by nuclear magnetic resonance. J Mol Biol 201: 637-657
43. Kagi JH (1991) Overview of metallothionein. Methods Enzymol 205: 613-626

44. Thirumoorthy N, Manisenthil Kumar KT, Shyam Sundar A et al (2007) Metallothionein: an overview. World J Gastroenterol 13: 993-996
45. Oz G, Pountney DL, Armitage IM (1999) In: Klaassen CD (ed) Metallothionein IV. Birkhauser Verlag Basel
46. Furey WF, Robbins AH, Clancy LL et al (1986) Crystal structure of Cd,Zn metallothionein. Science 231: 704-710
47. Palmiter RD, Findley SD, Whitmore TE et al (1992) MT-III, a brain-specific member of the metallothionein gene family. Proc Natl Acad Sci U S A 89: 6333-6337
48. Oz G, Zangger K, Armitage IM (2001) Three-dimensional structure and dynamics of a brain specific growth inhibitory factor: metallothionein-3. Biochemistry 40: 11433-11441
49. Blindauer CA (2008) Metallothioneins with unusual residues: histidines as modulators of zinc affinity and reactivity. J Inorg Biochem 102: 507-521
50. Berg JM, Shi Y (1996) The galvanization of biology: a growing appreciation for the roles of zinc. Science 271: 1081-1085
51. Lee MS, Gippert GP, Soman KV et al (1989) Three-dimensional solution structure of a single zinc finger DNA-binding domain. Science 245: 635-637
52. Stoll R, Lee BM, Debler EW et al (2007) Structure of the Wilms tumor suppressor protein zinc finger domain bound to DNA. J Mol Biol 372: 1227-1245
53. Cornilescu CC, Porter FW, Zhao KQ et al (2008) NMR structure of the mengovirus Leader protein zinc-finger domain. FEBS Lett 582: 896-900
54. Kotaka M, Johnson C, Lamb HK et al (2008) Structural analysis of the recognition of the negative regulator NmrA and DNA by the zinc finger from the GATA-type transcription factor AreA. J Mol Biol 381: 373-382
55. Chou CC, Lou YC, Tang TK et al (2010) Structure and DNA binding characteristics of the three-Cys(2)His(2) domain of mouse testis zinc finger protein. Proteins 78: 2202-2212
56. Brown RS (2005) Zinc finger proteins: getting a grip on RNA. Curr Opin Struct Biol 15: 94-98
57. Laity JH, Lee BM, Wright PE (2001) Zinc finger proteins: new insights into structural and functional diversity. Curr Opin Struct Biol 11: 39-46
58. Wolfe SA, Nekludova L, Pabo CO (2000) DNA recognition by Cys2His2 zinc finger proteins. Annu Rev Biophys Biomol Struct 29: 183-212
59. Lee S, Doddapaneni K, Hogue A et al (2010) Solution structure of Gfi-1 zinc domain bound to consensus DNA. J Mol Biol 397: 1055-1066
60. Eustermann S, Brockmann C, Mehrotra PV et al (2010) Solution structures of the two PBZ domains from human APLF and their interaction with poly(ADP-ribose). Nat Struct Mol Biol 17: 241-243
61. Isogai S, Kanno S, Ariyoshi M et al (2010) Solution structure of a zinc-finger domain that binds to poly-ADP-ribose. Genes Cells 15: 101-110
62. Hudson BP, Martinez-Yamout MA, Dyson HJ et al (2004) Recognition of the mRNA AU-rich element by the zinc finger domain of TIS11d. Nat Struct Mol Biol 11: 257-264

63. He Y, Imhoff R, Sahu A et al (2009) Solution structure of a novel zinc finger motif in the SAP30 polypeptide of the Sin3 corepressor complex and its potential role in nucleic acid recognition. Nucleic Acids Res 37: 2142-2152
64. He F, Umehara T, Saito K et al (2010) Structural insight into the zinc finger CW domain as a histone modification reader. Structure 18: 1127-1139
65. Watanabe S, Arai T, Matsumi R et al (2009) Crystal structure of HypA, a nickel-binding metallochaperone for [NiFe] hydrogenase maturation. J Mol Biol 394: 448-459
66. Cavalli A, Salvatella X, Dobson CM et al (2007) Protein structure determination from NMR chemical shifts. Proc Natl Acad Sci USA 104: 9615-9620
67. Shen Y, Lange O, Delaglio F et al (2008) Consistent blind protein structure generation from NMR chemical shift data. Proc Natl Acad Sci U S A 105: 4685-4690
68. Shen Y, Bryan PN, He Y et al (2010) De novo structure generation using chemical shifts for proteins with high-sequence identity but different folds. Protein Sci 19: 349-356
69. Raman S, Huang YJ, Mao B et al (2010) Accurate automated protein NMR structure determination using unassigned NOESY data. J Am Chem Soc 132: 202-207
70. Montalvao RW, Cavalli A, Salvatella X et al (2008) Structure determination of protein-protein complexes using NMR chemical shifts: case of an endonuclease colicin-immunity protein complex. J Am Chem Soc 130: 15990-15996
71. Oz G, Pountney DL, Armitage IM (1998) NMR spectroscopic studies of I = 1/2 metal ions in biological systems. Biochem Cell Biol 76: 223-234
72. Drakenberg T, Jaohansson C, Forsen S (1997) In: Reid DG (ed) Protein NMR techiniques. Human Press, Totowa, New Jersey
73. Sun H. 2002. Metallodrugs. In *Encyclopedia of Nuclear Magnetic Resonance: Advances in NMR*, ed. Grant DMaH, R.K., pp. 413-427. Chichester: John Wiley &Sons, Ltd
74. Blindauer CA, Harvey I, Bunyan KE et al (2009) Structure, properties, and engineering of the major zinc binding site on human albumin. J Biol Chem 284: 23116-23124
75. Li H, Otvos JD (1996) ^{111}Cd NMR studies of the domain specificity of Ag+ and Cu+ binding to metallothionein. Biochemistry 35: 13929-13936
76. Farrell RA, Thorvaldsen JL, Winge DR (1996) Identification of the Zn(II) site in the copper-responsive yeast transcription factor, AMT1: a conserved Zn module. Biochemistry 35: 1571-1580
77. Kakalis LT, Kennedy M, Sikkink R et al (1995) Characterization of the calcium-binding sites of calcineurin B. FEBS Lett 362: 55-58
78. Baleja JD, Marmorstein R, Harrison SC et al (1992) Solution structure of the DNA-binding domain of Cd2-GAL4 from S. cerevisiae. Nature 356: 450-453

79. Pan T, Coleman JE (1990) GAL4 transcription factor is not a "zinc finger" but forms a Zn(II)2Cys6 binuclear cluster. Proc Natl Acad Sci USA 87: 2077-2081
80. Vasak M (1998) Application of ^{113}Cd NMR to metallothioneins. Biodegradation 9: 501-512
81. Digilio G, Bracco C, Vergani L et al (2009) The cadmium binding domains in the metallothionein isoform Cd(7)-MT10 from Mytilus galloprovincialis revealed by NMR spectroscopy. J Biol Inorg Chem 14: 167-178
82. Serra-Batiste M, Cols N, Alcaraz LA et al (2010) The metal-binding properties of the blue crab copper specific CuMT-2: a crustacean metallothionein with two cysteine triplets. J Biol Inorg Chem 15: 759-776
83. Daniels MJ, Turner-Cavet JS, Selkirk R et al (1998) Coordination of Zn^{2+} (and Cd^{2+}) by prokaryotic metallothionein. Involvement of his-imidazole. J Biol Chem 273: 22957-22961
84. Stewart AJ, Blindauer CA, Berezenko S et al (2003) Interdomain zinc site on human albumin. Proc Natl Acad Sci USA 100: 3701-3706
85. Narula SS, Mehra RK, Winge DR et al (1991) Establishment of the metal-to-cysteine connectivities in silver-substituted yeast metallothionein. J Am Chem Soc 113: 9354-9358
86. Andersen RJ, diTargiani RC, Hancock RD et al (2006) Characterization of the first N2S(alkylthiolate)lead compound: a model for three-coordinate lead in biological systems. Inorg Chem 45: 6574-6576
87. Claudio ES, ter Horst MA, Forde CE et al (2000) ^{207}Pb-^{1}H two-dimensional NMR spectroscopy: a useful new tool for probing lead(II) coordination chemistry. Inorg Chem 39: 1391-1397
88. Aramini JM, Hiraoki T, Yazawa M et al (1996) Lead-207 NMR: A novel probe for the study of calcium-binding proteins. Journal of Biological Inorganic Chemistry 1: 39-48
89. Neupane KP, Pecoraro VL (2010) Probing a homoleptic PbS3 coordination environment in a designed peptide using ^{207}Pb NMR spectroscopy: implications for understanding the molecular basis of lead toxicity. Angew Chem Int Ed Engl 49: 8177-8180
90. DeSilva TM, Veglia G, Porcelli F et al (2002) Selectivity in heavy metal-binding to peptides and proteins. Biopolymers 64: 189-197
91. Iranzo O, Thulstrup PW, Ryu SB et al (2007) The application of ^{199}Hg NMR and (199m)Hg perturbed angular correlation (PAC) spectroscopy to define the biological chemistry of Hg(II): a case study with designed two- and three-stranded coiled coils. Chemistry 13: 9178-9190
92. Utschig LM, Wright JG, Dieckmann G et al (1995) The Hg-199 Chemical-Shift as a Probe of Coordination Environments in Blue Copper Proteins. Inorganic Chemistry 34: 2497-2498
93. Steele RA, Opella SJ (1997) Structures of the reduced and mercury-bound forms of MerP, the periplasmic protein from the bacterial mercury detoxification system. Biochemistry 36: 6885-6895

94. Utschig LM, Bryson JW, O'Halloran TV (1995) Mercury-199 NMR of the metal receptor site in MerR and its protein-DNA complex. Science 268: 380-385
95. Utschig LM, Baynard T, Strong C et al (1997) Probing Copper-Thioether Coordination Chemistry in Rusticyanin and Azurin by 2D ^{1}H-^{199}Hg NMR. Inorg Chem 36: 2926-2927
96. Huffman DL, Utschig LM, O'Halloran TV (1997) Mercury-responsive gene regulation and mercury-199 as a probe of protein structure. Met Ions Biol Syst 34: 503-526
97. Kornhaber GJ, Snyder D, Moseley HN et al (2006) Identification of zinc-ligated cysteine residues based on 13Calpha and 13Cbeta chemical shift data. J Biomol NMR 34: 259-269
98. Kostic M, Matt T, Martinez-Yamout MA et al (2006) Solution structure of the Hdm2 C2H2C4 RING, a domain critical for ubiquitination of p53. J Mol Biol 363: 433-450
99. Zuiderweg ER (2002) Mapping protein-protein interactions in solution by NMR spectroscopy. Biochemistry 41: 1-7
100. Gao G, Williams JG, Campbell SL (2004) Protein-protein interaction analysis by nuclear magnetic resonance spectroscopy. Methods Mol Biol 261: 79-92
101. Zeng YB, Zhang DM, Li H et al (2008) Binding of Ni^{2+} to a histidine- and glutamine-rich protein, Hpn-like. J Biol Inorg Chem 13: 1121-1131
102. Syme CD, Viles JH (2006) Solution ^{1}H NMR investigation of Zn^{2+} and Cd^{2+} binding to amyloid-beta peptide (Abeta) of Alzheimer's disease. Biochim Biophys Acta 1764: 246-256
103. Jones CE, Klewpatinond M, Abdelraheim SR et al (2005) Probing copper2+ binding to the prion protein using diamagnetic nickel2+ and 1H NMR: the unstructured N terminus facilitates the coordination of six copper2+ ions at physiological concentrations. J Mol Biol 346: 1393-1407
104. Jensen MR, Hass MA, Hansen DF et al (2007) Investigating metal-binding in proteins by nuclear magnetic resonance. Cell Mol Life Sci 64: 1085-1104
105. Schumann FH, Riepl H, Maurer T et al (2007) Combined chemical shift changes and amino acid specific chemical shift mapping of protein-protein interactions. J Biomol NMR 39: 275-289
106. Bertini I, Das Gupta S, Hu X et al (2009) Solution structure and dynamics of S100A5 in the apo and Ca^{2+}-bound states. J Biol Inorg Chem 14: 1097-1107
107. Banci L, Bertini I, Ciofi-Baffoni S et al (2008) A structural-dynamical characterization of human Cox17. J Biol Chem 283: 7912-7920
108. Banci L, Bertini I, Cantini F et al (2009) An NMR study of the interaction of the N-terminal cytoplasmic tail of the Wilson disease protein with copper(I)-HAH1. J Biol Chem 284: 9354-9360
109. Pelton JG, Torchia DA, Meadow ND et al (1993) Tautomeric states of the active-site histidines of phosphorylated and unphosphorylated IIIGlc, a signal-transducing protein from Escherichia coli, using two-dimensional heteronuclear NMR techniques. Protein Sci 2: 543-558

110. Lee BM, Buck-Koehntop BA, Martinez-Yamout MA et al (2007) Embryonic neural inducing factor churchill is not a DNA-binding zinc finger protein: solution structure reveals a solvent-exposed beta-sheet and zinc binuclear cluster. J Mol Biol 371: 1274-1289
111. Otting G (2010) Protein NMR using paramagnetic ions. Annu Rev Biophys 39: 387-405
112. Arnesano F, Banci L, Piccioli M (2005) NMR structures of paramagnetic metalloproteins. Q Rev Biophys 38: 167-219
113. Bertini I, Luchinat C, Rosato A (1996) The solution structure of paramagnetic metalloproteins. Prog Biophys Mol Biol 66: 43-80
114. Otting G (2008) Prospects for lanthanides in structural biology by NMR. J Biomol NMR 42: 1-9
115. Clore GM, Iwahara J (2009) Theory, practice, and applications of paramagnetic relaxation enhancement for the characterization of transient low-population states of biological macromolecules and their complexes. Chem Rev 109: 4108-4139
116. Iwahara J, Tang C, Marius Clore G (2007) Practical aspects of ^{1}H transverse paramagnetic relaxation enhancement measurements on macromolecules. J Magn Reson 184: 185-195
117. Bertini I, Ciurli S, Dikiy A et al (2001) The first solution structure of a paramagnetic copper(II) protein: the case of oxidized plastocyanin from the cyanobacterium Synechocystis PCC6803. J Am Chem Soc 123: 2405-2413
118. Ubbink M, Worrall JA, Canters GW et al (2002) Paramagnetic resonance of biological metal centers. Annu Rev Biophys Biomol Struct 31: 393-422
119. Hansen DF, Led JJ (2006) Determination of the geometric structure of the metal site in a blue copper protein by paramagnetic NMR. Proc Natl Acad Sci U S A 103: 1738-1743
120. Donaldson LW, Skrynnikov NR, Choy WY et al (2001) Structural characterization of proteins with an attached ATCUN motif by paramagnetic relaxation enhancement NMR spectroscopy. J Am Chem Soc 123: 9843-9847
121. Iwahara J, Schwieters CD, Clore GM (2004) Ensemble approach for NMR structure refinement against (1)H paramagnetic relaxation enhancement data arising from a flexible paramagnetic group attached to a macromolecule. J Am Chem Soc 126: 5879-5896
122. Yagi H, Loscha KV, Su XC et al (2010) Tunable paramagnetic relaxation enhancements by $[Gd(DPA)_3]^{3-}$ for protein structure analysis. J Biomol NMR 47: 143-153
123. Su XC, Otting G (2010) Paramagnetic labelling of proteins and oligonucleotides for NMR. J Biomol NMR 46: 101-112
124. Iwahara J, Schwieters CD, Clore GM (2004) Characterization of nonspecific protein-DNA interactions by 1H paramagnetic relaxation enhancement. J Am Chem Soc 126: 12800-12808
125. Fawzi NL, Doucleff M, Suh JY et al (2010) Mechanistic details of a protein-protein association pathway revealed by paramagnetic relaxation

enhancement titration measurements. Proc Natl Acad Sci USA 107: 1379-1384
126. Yu D, Volkov AN, Tang C (2009) Characterizing dynamic protein-protein interactions using differentially scaled paramagnetic relaxation enhancement. J Am Chem Soc 131: 17291-17297
127. Liang B, Bushweller JH, Tamm LK (2006) Site-directed parallel spin-labeling and paramagnetic relaxation enhancement in structure determination of membrane proteins by solution NMR spectroscopy. J Am Chem Soc 128: 4389-4397
128. Clore GM, Tang C, Iwahara J (2007) Elucidating transient macromolecular interactions using paramagnetic relaxation enhancement. Curr Opin Struct Biol 17: 603-616
129. Tang C, Schwieters CD, Clore GM (2007) Open-to-closed transition in apo maltose-binding protein observed by paramagnetic NMR. Nature 449: 1078-1082
130. Iwahara J, Clore GM (2006) Detecting transient intermediates in macromolecular binding by paramagnetic NMR. Nature 440: 1227-1230
131. Volkov AN, Ubbink M, van Nuland NA (2010) Mapping the encounter state of a transient protein complex by PRE NMR spectroscopy. J Biomol NMR 48: 225-236
132. Bertini I, Luchinat C, Parigi G (2002) Magnetic susceptibility in paramagnetic NMR. Prog. Nucl. Magn. Reson. Spectrosc. 40, 249-273
133. Biekofsky RR, Muskett FW, Schmidt JM et al (1999) NMR approaches for monitoring domain orientations in calcium-binding proteins in solution using partial replacement of Ca^{2+} by Tb^{3+}. FEBS Lett 460: 519-526
134. Banci L, Bertini I, Bren KL et al (1996) The use of peudocontact shifts to refine solution structures of paramagnetic metalloproteins: Met80Ala cyano-cytochrome c as an exampme. J Biol Inorg Chem 1: 117-126
135. Goodfellow BJ, Duarte IC, Macedo AL et al (2010) An NMR structural study of nickel-substituted rubredoxin. J Biol Inorg Chem 15: 409-420
136. Arnesano F, Banci L, Bertini I et al (2003) A strategy for the NMR characterization of type II copper(II) proteins: the case of the copper trafficking protein CopC from Pseudomonas Syringae. J Am Chem Soc 125: 7200-7208
137. Bertini I, Kursula P, Luchinat C et al (2009) Accurate solution structures of proteins from X-ray data and a minimal set of NMR data: calmodulin-peptide complexes as examples. J Am Chem Soc 131: 5134-5144
138. Pintacuda G, Park AY, Keniry MA et al (2006) Lanthanide labeling offers fast NMR approach to 3D structure determinations of protein-protein complexes. J Am Chem Soc 128: 3696-3702
139. Pintacuda G, John M, Su XC et al (2007) NMR structure determination of protein-ligand complexes by lanthanide labeling. Acc Chem Res 40: 206-212

140. Nguyen TH, Ozawa K, Stanton-Cook M et al (2010) Generation of Pseudocontact Shifts in Protein NMR Spectra with a Genetically Encoded Cobalt(II)-Binding Amino Acid. Angew Chem Int Ed Engl
141. Bertini I, Del Bianco C, Gelis I et al (2004) Experimentally exploring the conformational space sampled by domain reorientation in calmodulin. Proc Natl Acad Sci U S A 101: 6841-6846
142. Bertini I, Gupta YK, Luchinat C et al (2007) Paramagnetism-based NMR restraints provide maximum allowed probabilities for the different conformations of partially independent protein domains. J Am Chem Soc 129: 12786-12794
143. Bertini I, Duma L, Felli IC et al (2004) A heteronuclear direct-detection NMR spectroscopy experiment for protein-backbone assignment. Angewandte Chemie-International Edition 43: 2257-2259
144. Bermel W, Bertini I, Felli IC et al (2006) C-13-detected protonless NMR spectroscopy of proteins in solution. Progress in Nuclear Magnetic Resonance Spectroscopy 48: 25-45
145. Bertini I, Jimenez B, Pierattelli R et al (2008) Protonless ^{13}C direct detection NMR: characterization of the 37 kDa trimeric protein CutA1. Proteins 70: 1196-1205
146. Machonkin TE, Westler WM, Markley JL (2002) (13)C[(13)C] 2D NMR: a novel strategy for the study of paramagnetic proteins with slow electronic relaxation rates. J Am Chem Soc 124: 3204-3205
147. Caillet-Saguy C, Delepierre M, Lecroisey A et al (2006) Direct-detected 13C NMR to investigate the iron(III) hemophore HasA. J Am Chem Soc 128: 150-158
148. Balayssac S, Bertini I, Luchinat C et al (2006) ^{13}C direct detected NMR increases the detectability of residual dipolar couplings. J Am Chem Soc 128: 15042-15043
149. Bermel W, Bertini I, Felli IC et al (2003) ^{13}C direct detection experiments on the paramagnetic oxidized monomeric copper, zinc superoxide dismutase. J Am Chem Soc 125: 16423-16429
150. Andersson P, Weigelt J, Otting G (1998) Spin-state selection filters for the measurement of heteronuclear one-bond coupling constants. J Biomol NMR 12: 435-441
151. Ottiger M, Delaglio F, Bax A (1998) Measurement of J and dipolar couplings from simplified two-dimensional NMR spectra. J Magn Reson 131: 373-378
152. Duma L, Hediger S, Lesage A et al (2003) Spin-state selection in solid-state NMR. J Magn Reson 164: 187-195
153. Meissner A, Duus JO, Sørensen OW (1997) Integration of spin-state-selective excitation into 2D NMR correlation experiments with the heteronuclear ZQ/2Q pi rotations for $^{1}J_{XH}$- resolved E.COSY-type measurements of heteronuclear coupling constants in proteins. J Biomol NMR 10: 89-94

154. Bermel W, Bertini I, Duma L et al (2005) Complete assignment of heteronuclear protein resonances by protonless NMR spectroscopy. Angew Chem Int Ed Engl 44: 3089-3092
155. Bermel W, Bertini I, Felli IC et al (2006) Protonless NMR experiments for sequence-specific assignment of backbone nuclei in unfolded proteins. J Am Chem Soc 128: 3918-3919
156. Bertini I, Felli IC, Kummerle R et al (2004) ^{13}C-^{13}C NOESY: an attractive alternative for studying large macromolecules. J Am Chem Soc 126: 464-465
157. Bertini I, Felli IC, Kummerle R et al (2004) C-13-C-13 NOESY: A constructive use of C-13-C-13 spin-diffusion. Journal of Biomolecular Nmr 30: 245-251
158. Arnesano F, Banci L, Bertini I et al (2003) A redox switch in CopC: an intriguing copper trafficking protein that binds copper(I) and copper(II) at different sites. Proc Natl Acad Sci U S A 100: 3814-3819
159. Madl T, Felli IC, Bertini I et al (2010) Structural analysis of protein interfaces from ^{13}C direct-detected paramagnetic relaxation enhancements. J Am Chem Soc 132: 7285-7287
160. Babini E, Bertini I, Capozzi F et al (2004) Direct carbon detection in paramagnetic metalloproteins to further exploit pseudocontact shift restraints. J Am Chem Soc 126: 10496-10497
161. Bermel W, Bertini I, Felli IC et al (2010) Exclusively heteronuclear NMR experiments to obtain structural and dynamic information on proteins. Chemphyschem 11: 689-695
162. Kostic M, Pochapsky SS, Pochapsky TC (2002) Rapid recycle (13)C',(15)N and (13)C,(13)C' heteronuclear and homonuclear multiple quantum coherence detection for resonance assignments in paramagnetic proteins: example of Ni^{2+}-containing acireductone dioxygenase. J Am Chem Soc 124: 9054-9055
163. Bertini I, Jimenez B, Piccioli M et al (2005) Asymmetry in ^{13}C-^{13}C COSY spectra provides information on ligand geometry in paramagnetic proteins. J Am Chem Soc 127: 12216-12217
164. Turano P, Lalli D, Felli IC et al (2010) NMR reveals pathway for ferric mineral precursors to the central cavity of ferritin. Proc Natl Acad Sci USA 107: 545-550
165. Matzapetakis M, Turano P, Theil EC et al (2007) ^{13}C- ^{13}C NOESY spectra of a 480 kDa protein: solution NMR of ferritin. J Biomol NMR 38: 237-242
166. Williamson MP, Havel TF, Wuthrich K (1985) Solution conformation of proteinase inhibitor IIA from bull seminal plasma by ^{1}H nuclear magnetic resonance and distance geometry. J Mol Biol 182: 295-315
167. Kupce E, Freeman R (2008) Fast multi-dimensional NMR by minimal sampling. J Magn Reson 191: 164-168
168. Frueh DP, Sun ZY, Vosburg DA et al (2006) Non-uniformly sampled double-TROSY hNcaNH experiments for NMR sequential assignments of large proteins. J Am Chem Soc 128: 5757-5763

169. Marion D (2005) Fast acquisition of NMR spectra using Fourier transform of non-equispaced data. J Biomol NMR 32: 141-150
170. Szyperski T, Yeh DC, Sukumaran DK et al (2002) Reduced-dimensionality NMR spectroscopy for high-throughput protein resonance assignment. Proc Natl Acad Sci USA 99: 8009-8014
171. Felli IC, Brutscher B (2009) Recent advances in solution NMR: fast methods and heteronuclear direct detection. Chemphyschem 10: 1356-1368
172. Kim S, Szyperski T (2003) GFT NMR, a new approach to rapidly obtain precise high-dimensional NMR spectral information. J Am Chem Soc 125: 1385-1393
173. Freeman R, Kupce E (2003) New methods for fast multidimensional NMR. J Biomol NMR 27: 101-113
174. Kupce E, Freeman R (2004) Projection-reconstruction technique for speeding up multidimensional NMR spectroscopy. J Am Chem Soc 126: 6429-6440
175. Schanda P, Van Melckebeke H, Brutscher B (2006) Speeding up three-dimensional protein NMR experiments to a few minutes. J Am Chem Soc 128: 9042-9043
176. Schanda P, Brutscher B (2005) Very fast two-dimensional NMR spectroscopy for real-time investigation of dynamic events in proteins on the time scale of seconds. J Am Chem Soc 127: 8014-8015
177. Kupce E, Freeman R (2003) Fast multi-dimensional Hadamard spectroscopy. J Magn Reson 163: 56-63
178. Hiller S, Wasmer C, Wider G et al (2007) Sequence-specific resonance assignment of soluble nonglobular proteins by 7D APSY-NMR spectroscopy. J Am Chem Soc 129: 10823-10828
179. Shen Y, Atreya HS, Liu G et al (2005) G-matrix Fourier transform NOESY-based protocol for high-quality protein structure determination. J Am Chem Soc 127: 9085-9099
180. Hiller S, Garces RG, Malia TJ et al (2008) Solution structure of the integral human membrane protein VDAC-1 in detergent micelles. Science 321: 1206-1210
181. Tugarinov V, Kay LE, Ibraghimov I et al (2005) High-resolution four-dimensional ^{1}H-^{13}C NOE spectroscopy using methyl-TROSY, sparse data acquisition, and multidimensional decomposition. J Am Chem Soc 127: 2767-2775
182. Baldwin AJ, Kay LE (2009) NMR spectroscopy brings invisible protein states into focus. Nat Chem Biol 5: 808-814
183. Bermel W, Bertini I, Felli IC et al (2009) Speeding up ^{13}C direct detection biomolecular NMR spectroscopy. J Am Chem Soc 131: 15339-15345
184. Lipton AS, Heck RW, Staeheli GR et al (2008) A QM/MM approach to interpreting ^{67}Zn solid-state NMR data in zinc proteins. J Am Chem Soc 130: 6224-6230

185. Lipton AS, Heck RW, Primak S et al (2008) Characterization of Mg^{2+} binding to the DNA repair protein apurinic/apyrimidic endonuclease 1 via solid-state ^{25}Mg NMR spectroscopy. J Am Chem Soc 130: 9332-9341